bovis bacillus Calmette-Guérin peptidoglycan," *Infection and Immunity*, vol. 71, no. 8, pp. 4238–4249, 2003.

[10] J. M. Roda, R. Parihar, and W. E. Carson III, "CpG-containing oligodeoxynucleotides act through TLR9 to enhance the NK cell cytokine response to antibody-coated tumor cells," *Journal of Immunology*, vol. 175, no. 3, pp. 1619–1627, 2005.

[11] T. Kawashima, Y. Norose, Y. Watanabe et al., "Cutting edge: major CD8 T cell response to live bacillus Calmette-Guérin is mediated by CD1 molecules," *Journal of Immunology*, vol. 170, no. 11, pp. 5345–5348, 2003.

[12] N. P. Goonetilleke, H. McShane, C. M. Hannan, R. J. Anderson, R. H. Brookes, and A. V. S. Hill, "Enhanced immunogenicity and protective efficacy against *Mycobacterium tuberculosis* of bacille Calmette-Guérin vaccine using mucosal administration and boosting with a recombinant modified vaccinia virus Ankara," *Journal of Immunology*, vol. 171, no. 3, pp. 1602–1609, 2003.

[13] E. A. Ramsburg, J. M. Publicover, D. Coppock, and J. K. Rose, "Requirement for CD4 T cell help in maintenance of memory CD8 T cell responses is epitope dependent," *Journal of Immunology*, vol. 178, no. 10, pp. 6350–6358, 2007.

[14] Global Tuberculosis Control Report, 2010, http://whqlibdoc .who.int/publications/2010/9789241564069_eng.pdf.

[15] The Global Plan to Stop TB 2011–2015, pp 81-88, 2010, http://www.stoptb.org/global/plan.

[16] D. F. Hoft, A. Blazevic, G. Abate et al., "A new recombinant bacille Calmette-Guérin vaccine safely induces significantly enhanced tuberculosis-specific immunity in human volunteers," *Journal of Infectious Diseases*, vol. 198, no. 10, pp. 1491–1501, 2008.

[17] L. Grode, P. Seiler, S. Baumann et al., "Increased vaccine efficacy against tuberculosis of recombinant *Mycobacterium bovis* bacille Calmette-Guérin mutants that secrete listeriolysin," *Journal of Clinical Investigation*, vol. 115, no. 9, pp. 2472–2479, 2005.

[18] K. Von Eschen, R. Morrison, M. Braun et al., "The candidate tuberculosis vaccine Mtb72F/AS02A: tolerability and immunogenicity in humans," *Human Vaccines*, vol. 5, no. 7, pp. 475–482, 2009.

[19] J. T. van Dissel, S. M. Arend, C. Prins et al., "Ag85B-ESAT-6 adjuvanted with IC31 promotes strong and long-lived *Mycobacterium tuberculosis* specific T cell responses in naïve human volunteers," *Vaccine*, vol. 28, no. 20, pp. 3571–3581, 2010.

[20] H. McShane, A. A. Pathan, C. R. Sander et al., "Recombinant modified vaccinia virus Ankara expressing antigen 85A boosts BCG-primed and naturally acquired antimycobacterial immunity in humans," *Nature Medicine*, vol. 10, no. 11, pp. 1240–1244, 2004.

[21] B. Abel, M. Tameris, N. Mansoor et al., "The novel tuberculosis vaccine, AERAS-402, induces robust and polyfunctional CD4$^+$ and CD8$^+$ T cells in adults," *American Journal of Respiratory and Critical Care Medicine*, vol. 181, no. 12, pp. 1407–1417, 2009.

[22] T. J. Scriba, M. Tameris, N. Mansoor et al., "Modified vaccinia Ankara-expressing Ag85A, a novel tuberculosis vaccine, is safe in adolescents and children, and induces polyfunctional CD4+ T cells," *European Journal of Immunology*, vol. 40, no. 1, pp. 279–290, 2010.

[23] R. Sun, Y. A. W. Skeiky, A. Izzo et al., "Novel recombinant BCG expressing perfringolysin O and the over-expression of key immunodominant antigens; pre-clinical characterization, safety and protection against challenge with *Mycobacterium tuberculosis*," *Vaccine*, vol. 27, no. 33, pp. 4412–4423, 2009.

[24] UNAIDS Report on the Global AIDS Epidemic, 2010, http:// www.unaids.org/documents/20101123_GlobalReport_em.pdf.

[25] R. Granich, S. Crowley, M. Vitoria et al., "Highly active antiretroviral treatment as prevention of HIV transmission: review of scientific evidence and update," *Current Opinion in HIV and AIDS*, vol. 5, no. 4, pp. 298–304, 2010.

[26] A. E. Grulich, M. T. van Leeuwen, M. O. Falster, and C. M. Vajdic, "Incidence of cancers in people with HIV/AIDS compared with immunosuppressed transplant recipients: a meta-analysis," *Lancet*, vol. 370, no. 9581, pp. 59–67, 2007.

[27] K. A. Gebo, J. A. Fleishman, R. Conviser et al., "HIV Research Network. Contemporary costs of HIV healthcare in the HAART era," *AIDS*, vol. 24, no. 17, pp. 2705–2715, 2010.

[28] N. L. Letvin, D. H. Barouch, and D. C. Montefiori, "Prospects for vaccine protection against HIV-1 infection and AIDS," *Annual Review of Immunology*, vol. 20, pp. 73–99, 2002.

[29] S. H. E. Kaufmann and A. J. McMichael, "Annulling a dangerous liaison: vaccination strategies against AIDS and tuberculosis," *Nature Medicine*, vol. 11, no. 4, pp. S33–S44, 2005.

[30] N. L. Letvin, "Progress toward an HIV vaccine," *Annual Review of Medicine*, vol. 56, pp. 213–223, 2005.

[31] G. Pantaleo and R. A. Koup, "Correlates of immune protection in HIV-1 infection: what we know, what we don't know, what we should know," *Nature Medicine*, vol. 10, no. 8, pp. 806–810, 2004.

[32] M. Z. Smith and S. J. Kent, "Genetic influences on HIV infection: implications for vaccine development," *Sexual Health*, vol. 2, no. 2, pp. 53–62, 2005.

[33] A. S. Fauci, S. M. Schnittman, G. Poli, S. Koenig, and G. Pantaleo, "Immunopathogenic mechanisms in human immunodeficiency virus (HIV) infection," *Annals of Internal Medicine*, vol. 114, no. 8, pp. 678–693, 1991.

[34] A. J. McMichael and T. Hanke, "HIV vaccines 1983–2003," *Nature Medicine*, vol. 9, no. 7, pp. 874–880, 2003.

[35] M. D. Daniel, F. Kirchhoff, S. C. Czajak, P. K. Sehgal, and R. C. Desrosiers, "Protective effects of a live attenuated SIV vaccine with a deletion in the nef gene," *Science*, vol. 258, no. 5090, pp. 1938–1941, 1992.

[36] J. D. Lifson, M. Piatak, J. L. Rossio et al., "Whole inactivated SIV virion vaccines with functional envelope glycoproteins: safety, immunogenicity, and activity against intrarectal challenge," *Journal of Medical Primatology*, vol. 31, no. 4-5, pp. 205–216, 2002.

[37] J. S. James, "First AIDS vaccine tested did not protect, but gives scientific leads," *AIDS Treatment News*, no. 389, p. 6, 2003.

[38] D. P. Francis, W. L. Heyward, V. Popovic et al., "Candidate HIV/AIDS vaccines: Lessons learned from the world's first phase III efficacy trials," *AIDS*, vol. 17, no. 2, pp. 147–156, 2003.

[39] R. R. Amara and H. L. Robinson, "A new generation of HIV vaccines," *Trends in Molecular Medicine*, vol. 8, no. 10, pp. 489–495, 2002.

[40] R. R. Amara, F. Villinger, J. D. Altman et al., "Control of a mucosal challenge and prevention of AIDS by a multiprotein DNA/MVA vaccine," *Science*, vol. 292, no. 5514, pp. 69–74, 2001.

[41] I. Ourmanov, C. R. Brown, B. Moss et al., "Comparative efficacy of recombinant modified vaccinia virus Ankara expressing simian immunodeficiency virus (SIV) Gag-Pol and/or Env in macaques challenged with pathogenic SIV," *Journal of Virology*, vol. 74, no. 6, pp. 2740–2751, 2000.

[42] J. W. Shiver, T. M. Fu, L. Chen et al., "Replication-incompetent adenoviral vaccine vector elicits effective anti-immunodeficiency-virus immunity," *Nature*, vol. 415, no. 6869, pp. 331–335, 2002.

[43] M. S. Seaman, L. Xu, K. Beaudry et al., "Multiclade human immunodeficiency virus type 1 envelope immunogens elicit broad cellular and humoral immunity in rhesus monkeys," *Journal of Virology*, vol. 79, no. 5, pp. 2956–2963, 2005.

[44] T. Matano, M. Kobayashi, H. Igarashi et al., "Cytotoxic T lymphocyte-based control of simian immunodeficiency virus replication in a preclinical AIDS vaccine trial," *Journal of Experimental Medicine*, vol. 199, no. 12, pp. 1709–1718, 2004.

[45] J. Cohen, "Did Merck's failed HIV vaccine cause harm?" *Science*, vol. 318, no. 5853, pp. 1048–1049, 2007.

[46] S. Rerks-Ngarm, P. Pitisuttithum, S. Nitayaphan et al., "Vaccination with ALVAC and AIDSVAX to prevent HIV-1 infection in Thailand," *The New England Journal of Medicine*, vol. 361, no. 23, pp. 2209–2220, 2009.

[47] S. G. Hansen, C. Vieville, N. Whizin et al., "Effector memory T cell responses are associated with protection of rhesus monkeys from mucosal simian immunodeficiency virus challenge," *Nature Medicine*, vol. 15, no. 3, pp. 293–299, 2009.

[48] A. Aldovini and R. A. Young, "Humoral and cell-mediated immune responses to live recombinant BCG-HIV vaccines," *Nature*, vol. 351, no. 6326, pp. 479–482, 1991.

[49] Y. Yasutomi, S. Koenig, S. S. Haun et al., "Immunization with recombinant BCG-SIV elicits SIV-specific cytotoxic T lymphocytes in rhesus monkeys," *Journal of Immunology*, vol. 150, no. 7, pp. 3101–3107, 1993.

[50] Y. Yasutomi, S. Koenig, R. M. Woods et al., "A vaccine-elicited, single viral epitope-specific cytotoxic T lymphocyte response does not protect against intravenous, cell-free simian immunodeficiency virus challenge," *Journal of Virology*, vol. 69, no. 4, pp. 2279–2284, 1995.

[51] K. Matsuo, R. Yamaguchi, A. Yamazaki, H. Tasaka, and T. Yamada, "Cloning and expression of the *Mycobacterium bovis* BCG gene for extracellular α antigen," *Journal of Bacteriology*, vol. 170, no. 9, pp. 3847–3854, 1988.

[52] K. Matsuo, R. Yamaguchi, A. Yamazaki, H. Tasaka, K. Terasaka, and T. Yamada, "Cloning and expression of the gene for the cross-reactive α antigen of *Mycobacterium kansasii*," *Infection and Immunity*, vol. 58, no. 2, pp. 550–556, 1990.

[53] K. Matsuo, R. Yamaguchi, A. Yamazaki et al., "Establishment of a foreign antigen secretion system in mycobacteria," *Infection and Immunity*, vol. 58, no. 12, pp. 4049–4054, 1990.

[54] M. Honda, K. Matsuo, T. Nakasone et al., "Protective immune responses induced by secretion of a chimeric soluble protein from a recombinant *Mycobacterium bovis* bacillus Calmette-Guerin vector candidate vaccine for human immunodeficiency virus type 1 in small animals," *Proceedings of the National Academy of Sciences of the United States of America*, vol. 92, no. 23, pp. 10693–10697, 1995.

[55] I. Tagaya, T. Kitamura, and Y. Sano, "A new mutant of dermovaccinia virus," *Nature*, vol. 192, no. 4800, pp. 381–382, 1961.

[56] T. Kitamura, Y. Kitamura, and I. Tagaya, "Immunogenicity of an attenuated strain of vaccinia virus on rabbits and monkeys," *Nature*, vol. 215, no. 5106, pp. 1187–1188, 1967.

[57] K. Takeya, K. Nomoto, S. Muraoka, S. Shimotori, T. Taniguchi, and T. Miyake, "Growth of two strains of *Mycobacterium bovis* (BCG) in a thymic mice," *Journal of General Microbiology*, vol. 100, no. 2, pp. 403–405, 1977.

[58] K. Ishii, Y. Ueda, K. Matsuo et al., "Structural analysis of vaccinia virus DIs strain: application as a new replication-deficient viral vector," *Virology*, vol. 302, no. 2, pp. 433–444, 2002.

[59] K. Someya, K-Q Xin, K. Matsuo, K. Okuda, N. Yamamoto, and M. Honda, "A consecutive priming-boosting vaccination of mice with simian immunodeficiency virus (SIV) gag/pol DNA and recombinant vaccinia virus strain DIs elicits effective anti-SIV immunity," *Journal of Virology*, vol. 78, no. 18, pp. 9842–9853, 2004.

[60] K. Shinohara, K. Sakai, S. Ando et al., "A highly pathogenic simian/human immunodeficiency virus with genetic changes in cynomolgus monkey," *Journal of General Virology*, vol. 80, no. 5, pp. 1231–1240, 1999.

[61] Y. Ami, Y. Izumi, K. Matsuo et al., "Priming-boosting vaccination with recombinant *Mycobacterium bovis* bacillus Calmette-Guérin and a nonreplicating vaccinia virus recombinant leads to long-lasting and effective immunity," *Journal of Virology*, vol. 79, no. 20, pp. 12871–12879, 2005.

[62] M. J. Cayabyab, B. Korioth-Schmitz, Y. Sun et al., "Recombinant *Mycobacterium bovis* BCG prime-recombinant adenovirus boost vaccination in rhesus monkeys elicits robust polyfunctional simian immunodeficiency virus-specific T-cell responses," *Journal of Virology*, vol. 83, no. 11, pp. 5505–5513, 2009.

[63] M. Rosario, J. Fulkerson, S. Soneji et al., "Safety and immunogenicity of novel recombinant BCG and modified vaccinia virus Ankara vaccines in neonate rhesus macaques," *Journal of Virology*, vol. 84, no. 15, pp. 7815–7821, 2010.

[64] S. André, B. Seed, J. Eberle, W. Schraut, A. Bültmann, and J. Haas, "Increased immune response elicited by DNA vaccination with a synthetic gp120 sequence with optimized codon usage," *Journal of Virology*, vol. 72, no. 2, pp. 1497–1503, 1998.

[65] M. Uchijima, A. Yoshida, T. Nagata, and Y. Koide, "Optimization of codon usage of plasmid DNA vaccine is required for the effective MHC class I-restricted T cell responses against an intracellular bacterium," *Journal of Immunology*, vol. 161, no. 10, pp. 5594–5599, 1998.

[66] D. L. Narum, S. Kumar, W. O. Rogers et al., "Codon optimization of gene fragments encoding Plasmodium falciparum merzoite proteins enhances DNA vaccine protein expression and immunogenicity in mice," *Infection and Immunity*, vol. 69, no. 12, pp. 7250–7253, 2001.

[67] M. Kanekiyo, K. Matsuo, M. Hamatake et al., "Mycobacterial codon optimization enhances antigen expression and virus-specific immune responses in recombinant *Mycobacterium bovis* bacille Calmette-Guérin expressing human immunodeficiency virus type 1 Gag," *Journal of Virology*, vol. 79, no. 14, pp. 8716–8723, 2005.

[68] M. Kanekiyo, Y. Ami, K. Matsuo et al., "A low-dose codon-optimized recombinant BCG-based HIV vaccine: prime-boost vaccination with recombinant BCG and replication-defective recombinant vaccinia virus DIs evokes SIV-specific immunity which overcomes the anamnestic BCG immunity in macaques," in *Proceedings of the 16th International AIDS Conference*, Toronto, Canada, August 2006.

[69] C. K. Stover, G. P. Bansal, M. S. Hanson et al., "Protective immunity elicited by recombinant bacille Calmette-Guerin (BCG) expressing outer surface protein A (OspA) lipoprotein: a candidate Lyme disease vaccine," *Journal of Experimental Medicine*, vol. 178, no. 1, pp. 197–209, 1993.

[70] R. Edelman, K. Palmer, K. G. Russ et al., "Safety and immunogenicity of recombinant Bacille Calmette-Guerin (rBCG) expressing Borrelia burgdorferi outer surface protein A (OspA) lipoprotein in adult volunteers: a candidate Lyme disease vaccine," *Vaccine*, vol. 17, no. 7-8, pp. 904–914, 1999.

[71] S. Matsumoto, H. Yukitake, H. Kanbara, and T. Yamada, "Recombinant *Mycobacterium bovis* bacillus Calmette-Guerin secreting merozoite surface protein 1 (MSP1) induces protection against rodent malaria parasite infection depending on MSP1-stimulated interferon γ and parasite-specific antibodies," *Journal of Experimental Medicine*, vol. 188, no. 5, pp. 845–854, 1998.

[72] C. Zheng, P. Xie, and Y. Chen, "Recombinant *Mycobacterium bovis* BCG producing the circumsporozoite protein of Plasmodium falciparum FCC-1/HN strain induces strong immune responses in BALB/c mice," *Parasitology International*, vol. 51, no. 1, pp. 1–7, 2002.

[73] Y. D. Zhu, G. Fennelly, C. Miller et al., "Recombinant bacille Calmette-Guérin expressing the measles virus nucleoprotein protects infant rhesus macaques from measles virus pneumonia," *Journal of Infectious Diseases*, vol. 176, no. 6, pp. 1445–1453, 1997.

[74] S. Uno-Furuta, K. Matsuo, S. Tamaki et al., "Immunization with recombinant Calmette-Guerin bacillus (BCG)-hepatitis C virus (HCV) elicits HCV-specific cytotoxic T lymphocytes in mice," *Vaccine*, vol. 21, no. 23, pp. 3149–3156, 2003.

Spatial Configuration of Hepatitis E Virus Antigenic Domain[∇]

Li Xing,[1,2]† Joseph C. Wang,[1]† Tian-Cheng Li,[3] Yasuhiro Yasutomi,[4] James Lara,[5] Yury Khudyakov,[5]
Darren Schofield,[6] Suzanne U. Emerson,[6] Robert H. Purcell,[6] Naokazu Takeda,[3]
Tatsuo Miyamura,[3] and R. Holland Cheng[1]*

*Molecular and Cellular Biology, University of California, Davis, California 95616[1]; Karolinska Institute Structural Virology,
F68 University Hospital, SE-14186 Stockholm, Sweden[2]; Department of Virology II, National Institute of Infectious Disease,
Tokyo 162, Japan[3]; Tsukuba Primate Research Center, National Institute of Biomedical Innovation, Ibaraki 305-0843,
Japan[4]; Division of Viral Hepatitis, Centers for Disease Control and Prevention (CDC), Atlanta,
Georgia 30333[5]; and Hepatitis Virus Section, National Institute of Allergy and
Infectious Diseases, Bethesda, Maryland 208892[6]*

Hepatitis E virus (HEV) is a human pathogen that causes acute hepatitis. When an HEV capsid protein containing a 52-amino-acid deletion at the C terminus and a 111-amino-acid deletion at the N terminus is expressed in insect cells, the recombinant HEV capsid protein can self-assemble into a T=1 virus-like particle (VLP) that retains the antigenicity of the native HEV virion. In this study, we used cryoelectron microscopy and image reconstruction to show that anti-HEV monoclonal antibodies bind to the protruding domain of the capsid protein at the lateral side of the spikes. Molecular docking of the HEV VLP crystal structure revealed that Fab224 covered three surface loops of the recombinant truncated second open reading frame (ORF2) protein (PORF2) at the top part of the spike. We also determined the structure of a chimeric HEV VLP and located the inserted B-cell tag, an epitope of 11 amino acids coupled to the C-terminal end of the recombinant ORF2 protein. The binding site of Fab224 appeared to be distinct from the location of the inserted B-cell tag, suggesting that the chimeric VLP could elicit immunity against both HEV and an inserted foreign epitope. Therefore, the T=1 HEV VLP is a novel delivery system for displaying foreign epitopes at the VLP surface in order to induce antibodies against both HEV and the inserted epitope.

Hepatitis E virus (HEV) is a causative agent of acute hepatitis in humans and is primarily transmitted via the fecal-oral route. HEV is thus resistant to the low pH and digestive enzymes associated with the stomach and gastrointestinal tract. HEV regularly causes epidemics in many tropical and subtropical countries. In India, 101 outbreaks were confirmed by serological analysis in the state of Maharashtra in the last 5 years (6), and the lifetime risk of HEV infection exceeds 60% (28). Sporadic cases have also been reported in regions where HEV is endemic, as well as in areas where it is not endemic. Although some of these cases were associated with travel, many cases involved patients without a history of travel to regions where HEV is endemic. Accumulating evidence suggests that sporadic infection occurs through a zoonotic route and is not limited to developing countries. Seroprevalence suggests hepatitis E infection may also be prevalent in high-income countries (21), such as the United States (17), the United Kingdom (3), and Japan (18). The overall mortality rate of HEV infection during an outbreak generally ranges from 1 to 15%, and the highest mortality occurs in pregnant women, with fatality rates of up to 30% (19).

The HEV virion is composed of a 7.2-kb single-stranded RNA molecule and a 32- to 34-nm icosahedral capsid. The HEV genome contains three open reading frames (ORFs).

The capsid protein, encoded by the second open reading frame (ORF2), located at the 3' terminus of the genome, comprises 660 amino acids and is responsible for most capsid-related functions, such as assembly, host interaction, and immunogenicity. Recombinant ORF2 proteins can induce antibodies that block HEV infection in nonhuman primates (12, 27). Four major antigenic domains were predicted to be located within the C-terminal 268 amino acids of the ORF2 protein; one domain was experimentally identified as a neutralization epitope in the Sar-55 ORF2 capsid protein (25, 26). However, the minimal peptide needed to induce anti-HEV neutralizing antibodies contains residues 459 to 607 of the ORF2 protein (33), which is much longer than a linear antigenic epitope, suggesting that the neutralization epitope is conformational. Therefore, the detailed structure of the HEV capsid protein is required in order to understand the organization of HEV epitopes.

Currently, there are 1,600 HEV genomic sequences available through the International Nucleotide Sequence Database Collaboration. They are classified into four genotypes which vary by geographic distribution and host range (10). In contrast, only a single serotype has been identified, suggesting that the immunodominant domain of HEV is highly conserved among genotypes. Antibodies from any one of the four genotypes cross-react with the capsid protein of genotype 1 (7).

Like other hepatitis viruses, HEV does not propagate well in currently available cell culture systems. Hepatitis E preventive strategies so far rely on the use of ORF2-derived recombinant protein (16). When expressed in insect cells, recombinant truncated ORF2 protein (PORF2), with 52 residues deleted from

* Corresponding author. Mailing address: Molecular and Cellular Biology, University of California, 1 Shields Ave., Davis, CA 95616. Phone: (530) 752-5659. Fax: (530) 752-3085. E-mail: rhch@ucdavis.edu.
† These authors contributed equally.
∇ Published ahead of print on 10 November 2010.

the C terminus and 111 residues deleted from the N terminus, self-assembles into virus-like particles (VLPs) (15). Our previous structural analysis of recombinant HEV VLP by cryoelectron microscopy (cryo-EM) provided the first understanding of the quaternary arrangement of PORF2.

The essential assembly element of the PORF2 protein contained amino acids 125 to 600 (13), and the reconstructed VLP displayed a T=1 icosahedral particle composed of 60 copies of truncated PORF2 (30). Recently, crystal structures were reported for genotype 1 T=1 VLPs (31), genotype 3 T=1 VLPs (32), and genotype 4 T=1 VLPs (8), revealing that PORF2 is composed of three domains, the S domain, M domain, and P domain. The T=1 icosahedral shell is composed of 60 copies of S domains, while the M domain binds tightly to the S domain and interacts with two 3-fold-related M domains to form a surface plateau at each of the 3-fold axes. Two P domains are tightly associated as a dimeric spike that protrudes from each of the icosahedral 2-fold axes. As a result, on a low-resolution cryo-EM density map, the HEV T=1 VLP appears as an icosahedral particle with 30 spikes (30).

Although these VLPs are smaller (270 Å in diameter) than the native HEV virion (320 to 340 Å), oral administration of HEV VLPs to experimental animals can induce anti-HEV antibodies that bind to native HEV (14). When a B-cell tag of 11 amino acids on glycoprotein D of herpes simplex virus was covalently coupled to the C-terminal end of PORF2 (after residue 608), the fusion protein retained the ability of PORF2 to assemble and form chimeric T=1 icosahedral VLPs that were capable of eliciting systemic and mucosal antibodies against both HEV capsid protein and the attached B-cell tag (20). Therefore, the HEV T=1 VLP is a potential carrier for delivering not only HEV antigen but also foreign antigens or antiviral drugs to the host immune system. However, rational design of HEV-based delivery vectors requires detailed information on HEV VLP structure, as well as on HEV immunodominant domains.

Here, we identified antigenic structures using cryo-EM and three-dimensional reconstruction. Our results indicate that the binding footprint of a neutralizing antibody covers the lateral side of the P domain, while a B-cell tag at the C terminus does not alter the assembly of T=1 HEV VLP.

MATERIALS AND METHODS

Production and purification of anti-HEV monoclonal antibody (MAb) MAb224. Eight-week-old female BALB/c mice were immunized at 0 and 4 weeks by intraperitoneal inoculation with HEV VLPs (100 μg/ml). Four weeks later, a final boost containing an equal volume of antigen was administered. Three days after the final boost, mouse spleen cells were fused with P3U1 mouse myeloma cells using polyethylene glycol 1500 (50% [wt/vol]) (Boehringer, Mannheim, Germany) essentially as described by Adler and Faine (1). Supernatants from microplate wells positive for hybridoma growth were screened by enzyme-linked immunosorbent assay (ELISA) using recombinant HEV VLP as the antigen. Hybridomas that secrete antibodies specific for HEV were subcloned three times by limiting dilution, after which they were considered to be monoclonal. Antibodies in the supernatants were isotyped using a mouse monoclonal antibody isotyping kit (Amersham, Little Chalfont, Buckinghamshire, United Kingdom) in accordance with the manufacturer's protocol. Hybridomas were grown in bulk in stationary flasks (Nunc, Roskilde, Denmark) using RPMI 1640 with 15% fetal calf serum. Antibodies were purified from cell supernatants using HiTrap protein G affinity columns (Pharmacia Biotech AB, Uppsala, Sweden) and stored at −80°C. Among all of the antibodies that were generated, MAb224, an immunoglobulin G1 (IgG1) isotype, was chosen for structural analysis.

Preparation of Fab224 fragments. Isolated Fab224 fragments were prepared from purified mouse monoclonal antibodies by papain cleavage. A reducing L-cysteine buffer was used to activate the papain, and MAb224 was mixed with papain at a molar ratio of 100:1. The mixture was incubated overnight at 30°C. The reaction was stopped by the addition of iodoacetamide, and the product was analyzed by SDS-PAGE. The Fab224 fragments were purified using a 5-ml prepacked protein A chromatography column (Pierce Protein Research) according to the manufacturer's instructions. The Fc fragments and uncleaved MAb224 antibodies were trapped in the column due to their affinity for protein A, while the Fab224 fragments were collected in the flowthrough fraction.

Production and purification of anti-HEV Fab4. Fab4 was prepared by phage display and purified according to the protocol described previously (25). Briefly, chimpanzee 1441 was infected with HEV strain SAR-55. Bone marrow was aspirated from the iliac crest of this animal, and the antibody κ-chain gene and γ1-chain gene were amplified and cloned into the pComb3H phage display vector and pGEM-T cloning vector (Promega), respectively, and transformed into *Escherichia coli* XL-1 Blue. The bacteria were then amplified and infected with helper phage VCS M13 at a multiplicity of infection of 50 to produce a library displayed on the surfaces of phage particles. Phage was panned on SAR-55 ORF2-coated ELISA wells; four rounds of panning were performed. After amplification of the selected library, the phagemid DNA was extracted and the vector was modified to remove the bacteriophage coat protein III-encoding region of the phage. The phagemid DNAs were religated and transformed into *E. coli* XL-1 Blue to produce soluble Fabs. The vector pComb3H was constructed to encode a six-histidine tail at the end of the Fab fragment, thus facilitating Fab purification. Fab4 purity was determined by SDS-PAGE, followed by colloidal Coomassie brilliant blue staining.

Production and purification of HEV VLPs. The production and purification of HEV VLPs were conducted as described previously (13, 15, 20, 30). Briefly, DNA fragments encoding the N-truncated ORF2 protein (for the wild-type VLP) and the chimeric ORF2 protein (for VLP-C-tag) were cloned using the baculovirus transfer vector pVL1393 to yield pVLORF2. Insect Sf9 cells (Riken Cell Bank, Tsukuba, Japan) were used to produce recombinant baculovirus. Tn5 insect cells were infected with the recombinant baculoviruses at a multiplicity of infection of 5 and incubated in Ex-Cell 405 medium (JRH Biosciences, Lenexa, KS) for 6 days at 26.5°C. The supernatant was collected after the removal of cell debris by centrifugation at 10,000 × g for 90 min. The HEV VLPs were pelleted at 100,000 × g for 2 h in a Beckman SW32 Ti rotor and resuspended in 4.5 ml Ex-Cell 405. The VLPs were further purified by centrifugation through a CsCl density gradient (1.31 g/ml) at 110,000 × g for 24 h at 4°C in a Beckman SW 55 Ti rotor. The white virus band was collected and diluted 4 times with Ex-Cell 405 to decrease the CsCl concentration, and then the VLPs were centrifuged for 2 h in a Beckman TLA 55 rotor at 100,000 × g. The VLPs were resuspended in 100 to 500 μl of 10 mM potassium-MES (morpholineethanesulfonic acid) buffer (pH = 6.2) and stored at 4°C. To construct chimeric VLP-C-tag, recombinant baculoviruses were prepared by inserting the B-cell tag epitope from herpes simplex virus glycoprotein D (QPELAPEDPED) at amino acid position 608 (20).

Western blotting. A series of DNA fragments were constructed to encode truncated ORF2 residues 112 to 660, 112 to 608, 112 to 602, 112 to 601, 112 to 600, 112 to 596, and 112 to 589. These recombinant ORF2 genes were inserted into a baculovirus vector and expressed in insect cells using the protocol for VLP production, except that the recombinant proteins were recovered from the cytoplasm after lysis of the cell. Recombinant proteins were heated in 4× Laemmli sample buffer and electrophoresed under reducing conditions in a 10% SDS–polyacrylamide gel. After transfer of proteins to a polyvinylidene difluoride (PVDF) membrane, the membrane was blocked with TBS buffer (20 mM Tris, pH 7.6, NaCl) containing 0.5% Tween 20 (vol/vol) prior to overnight incubation with Fab224 fragments at a 1:10 dilution. After extensive washing with TBS buffer containing 0.05% Tween 20 (vol/vol), alkaline phosphatase-conjugated anti-mouse IgG (Fab specific) was incubated with the membrane for 1 h at room temperature. The blot was then washed and developed with the *p*-nitroblue tetrazolium-5-bromo-4-chloro-3-indolylphosphate (NBT-BCIP) reaction.

Preparation of VLP-Fab complexes for cryoelectron microscopy. The VLP-Fab complexes were prepared by incubating Fabs with VLPs at a molar ratio exceeding 1:300 (VLP versus Fabs) at 4°C overnight. To reduce the background density in the subsequent structural determination, highly pure VLP-Fab complexes were obtained using a short column containing Sephacryl 300, which resulted in the removal of the unbound Fab from the sample. The fractions containing VLP-Fab complexes were collected based on their optical density readings at a wavelength of 280 nm. The Fab binding occupancy was roughly estimated by performing SDS-PAGE (8-to-25% gradient) on the purified VLP-Fab complexes at a constant voltage using the Phast system (Pharmacia). The

particle morphology of VLP-Fab complexes was examined by negative-stain electron microscopy using 2% uranyl acetate.

Cryoelectron microscopy. Sample preparation and cryo-EM were performed following previously described, well-established procedures (13, 30). Briefly, a drop containing 3.5 μl of the sample was applied to a glow-discharged holey carbon-coated copper grid, blotted with a piece of filter paper for 3 s to remove the extra liquid, and quickly plunged into liquid ethane cooled by liquid nitrogen. Samples were frozen in a thin layer of vitrified ice. The grid was then transferred into a Gatan 626DH cryo holder and kept at a low temperature (−178°C) during the subsequent data collection. Micrographs were collected under low-dose conditions (<10 $e^-/Å^2$) using Kodak SO163 film at a magnification of ×45,000 on an FEI CM-120 electron microscope operated at 120 kV, and particles were photographed at a defocus range of 1,000 to 3,000 nm. Micrographs were visually inspected and selected based on a suitable particle concentration, optimal ice thickness, and minimal specimen drift. Only micrographs fulfilling these criteria were analyzed.

Image processing. Selected micrographs were digitized using a Heidelberg Primescan D8200 (Heidelberg, Germany) at a 14-μm scanning step size, corresponding to 3.11 Å per pixel of specimen space. Particles were manually picked and centered by cross-correlating each one against the circular average image. The astigmatism and defocus value were evaluated by the superimposed power spectra from all particles within a single micrograph. The contrast transfer function's first zero was approximately within the range of 17 to 20 $Å^{-1}$ for the data used for the structural determination. The self-common-lines algorithm (4) was used to yield the initial models for VLP-C-tag, VLP-Fab4, and VLP-Fab224. The origin and orientation search for each particle was carried out iteratively using the polar Fourier transformation (PFT) algorithm running on an AMD MP1800 MHz dual-processor Linux workstation (2). Three-dimensional reconstructions were computed by combining a set of particles with orientations that spread evenly in an icosahedral asymmetric unit using the Fourier-Bessel algorithm and by superimposing 5-3-2 icosahedral symmetry. To examine the reliability of the three-dimensional reconstruction, the data set was evenly divided into two parts at the final refinement step and two three-dimensional reconstructions were computed. The resolution was estimated using Fourier shell correlation (FSC) by assessing the agreement between these two reconstructions in Fourier space. Using a coefficient value of 0.5 as the criteria, the estimated resolutions of the three-dimensional reconstructions of VLP-C-tag, VLP-Fab224, and VLP-Fab4 were computed as 17.5 Å, 18.5 Å, and 24 Å, respectively.

The three-dimensional reconstructions were rendered and visualized using the Chimera program (22). The contour level was chosen at a value corresponding to 100% of the mass of the PORF2 protein. The electron density map was displayed in the isosurface mode, which builds a barrier to contour the density about a certain threshold.

Fitting the crystal structure into cryo-EM density maps. The density of the bound Fab molecule was determined from a difference density map, which was calculated by subtracting the cryo-EM map of unbound HEV T=1 VLP from the density map of the Fab-VLP complex. The cryo-EM map of unbound HEV VLP was published previously (30). Because the cryo-EM data for unbound VLP and the Fab-VLP complex were collected with the same FEI CM-120 electron microscope under similar imaging conditions, the difference density map was calculated by direct subtraction of the density of unbound VLP from the reconstruction of the Fab-VLP complex after normalizing the contrast between the two maps. The calculated difference map was used as a constraint in model fitting. Manual fitting was carried out by translational and rotational movement of the three-dimensional crystal structure of the PORF2 protein (PDB ID 2ZZQ) (31) into the cryo-EM density maps using program O (9). To obtain the best fit, the atomic model of the PORF2 subunit was treated as a rigid body. The fitting was first manually refined by minimizing the crashes between symmetry-related PORF2 molecules and then evaluated based on the cross correlation coefficient (CC value) between the cryo-EM density and the density computed from the fitted PORF2 coordinates. Fitting was halted when the CC value reached 80%. The figures were prepared using the program PyMOL (5), and the surface stereographic projection of the HEV VLP was prepared using the program RIVEM (29).

RESULTS

Binding of antibody MAb224 to PORF2. The binding of the monoclonal antibody Fab224 to PORF2 was examined via immunoblot analysis. A series of recombinant ORF2 proteins with C-terminal truncations were separated by SDS-PAGE on
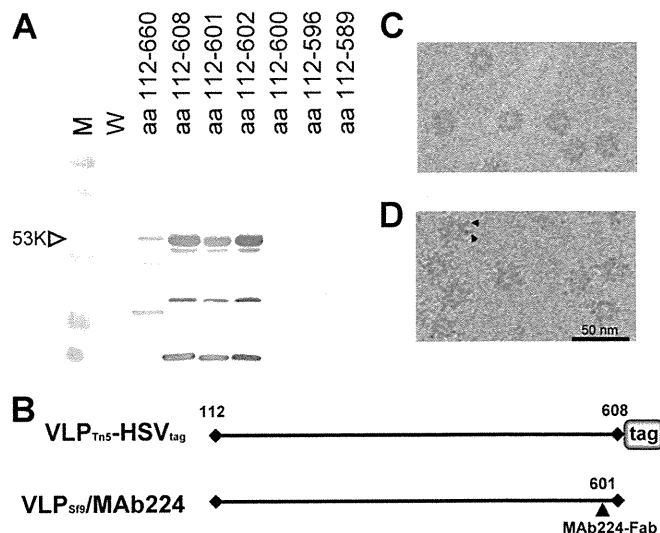

FIG. 1. Characterization of VLP-C-tag and VLP-Fab224. (A) Western blot assay of the C-terminally truncated ORF2 proteins with Fab224. M, molecular weight markers; W, peptides recovered from baculovirus-infected cells. (B) Diagram of the C-terminal markers. (C) Electron micrograph of frozen-hydrated VLP-C-tag. (D) Electron micrograph of frozen-hydrated VLP-Fab224. Black arrowheads indicate the Fab molecules attached to the VLP. Both particles showed an absence of density in the center. Note that the surface spikes in VLP-Fab224 appeared as longer thorn-like densities compared to those of VLP-C-tag.

a 10% gel under reducing conditions and blotted with Fab224 (Fig. 1A). Fab224 recognized both reduced and denatured recombinant ORF2 proteins that contained amino acids 112 to 660, 112 to 608, 112 to 602, and 112 to 601. In contrast, recombinant ORF2 proteins composed of residues 112 to 600, 112 to 596, and 112 to 589 did not bind to Fab224. These data indicate that residues 597 to 601 are critical for Fab224 binding to PORF2. Because the recombinant ORF2 proteins were recovered from cell cytoplasm where multiple forms of PORF2 were reported (15), the positive bands observed at a low molecular weight may be the proteolytic products or degraded forms of ORF2 that contain the Fab224 binding sequence.

Two-dimensional electron cryomicrographs. The chimeric VLPs (Fig. 1C) and the Fab224-conjugated VLP complex (Fig. 1D) showed circular profiles with spike-like densities that extended from the surface. As we observed previously (15, 30), they appeared to have a white, contrasting center, indicating that they are empty particles lacking RNA (data not shown). The sizes of both VLPs were approximately 27 nm without taking into account the extra densities that extended from the VLP-Fab224 surface (Fig. 1D).

Binding site of antibodies. The cryo-EM structure of HEV-Fab224 was reconstructed from 615 images of individual particles and displayed T=1 icosahedral symmetry with 60 protein subunits that were arranged into 30 dimeric protruding spikes located at each icosahedral 2-fold axis (Fig. 2A). Sixty Fab molecules were observed around each VLP particle, bound to the shoulder of the P domain. The Fab density extended ~57 Å radially away from the spike surface. The density corresponding to the Fab was approximately equal in magnitude to that of the HEV VLP, indicating that most or all of the 60

A

B

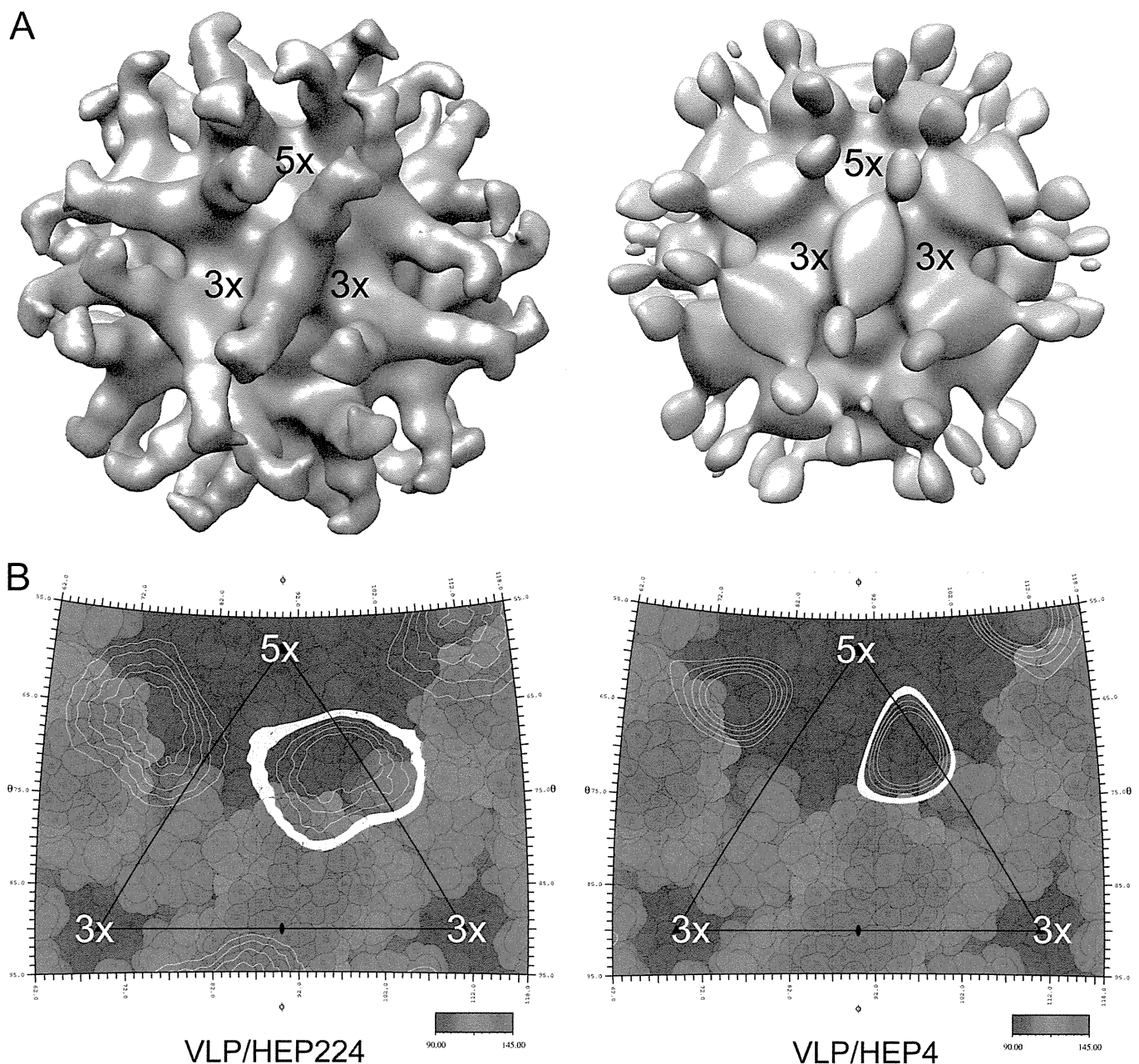VLP/HEP224   VLP/HEP4

FIG. 2. The cryo-EM structure of HEV T=1 VLP in complex with anti-HEV antibodies. (A) Surface presentation of VLP-Fab224 (left) and VLP-Fab4 (right) viewed along one of the icosahedral 2-fold axes. One 5-fold axis and two adjacent 3-fold axes are marked with the corresponding number. In both reconstructions, 60 copies of Fab are attached to the lateral side of HEV VLP; however, the density of Fab4 molecules appears to be less than that of Fab224 molecules. (B) The viral surface is shown as a stereographic projection overlapped with a line drawing of an icosahedral asymmetric unit. The 5-fold and two adjacent 3-fold axes are marked with corresponding numbers, while the black triangle encloses the area of an icosahedral asymmetric unit. The surface residues are colored according to the distance from the center of the VLP, with red being the furthest away and blue representing the surface depressions. The Fab density is projected as white contour lines on the viral surface, and the outermost layer of density is drawn as thick white contour lines.

binding sites were occupied by a Fab molecule. The density corresponding to the VLP capsid was removed from the cryo-EM map, producing a Fab differential density map that was used to pinpoint the binding site of the Fab224 antibody (Fig. 3A and B).

In addition, the structure of HEV VLP in complex with the neutralizing antibody Fab4 was determined by combining 264 individual images. Fab4 precipitates both the native HEV virion and recombinant PORF2 peptides, but the reaction depends on the presence of amino acids 597 to 607 (26). Three-dimensional reconstruction of the VLP-Fab4 complex showed 60 Fab molecules bound to each HEV VLP. Unlike the VLP-Fab224 complex, the density corresponding to Fab4 was about one-third of that of the capsid (Fig. 2A), suggesting that only 30 to 40% of the binding sites were occupied by the Fab. Moreover, the binding of Fab4 appeared to be deeper on the
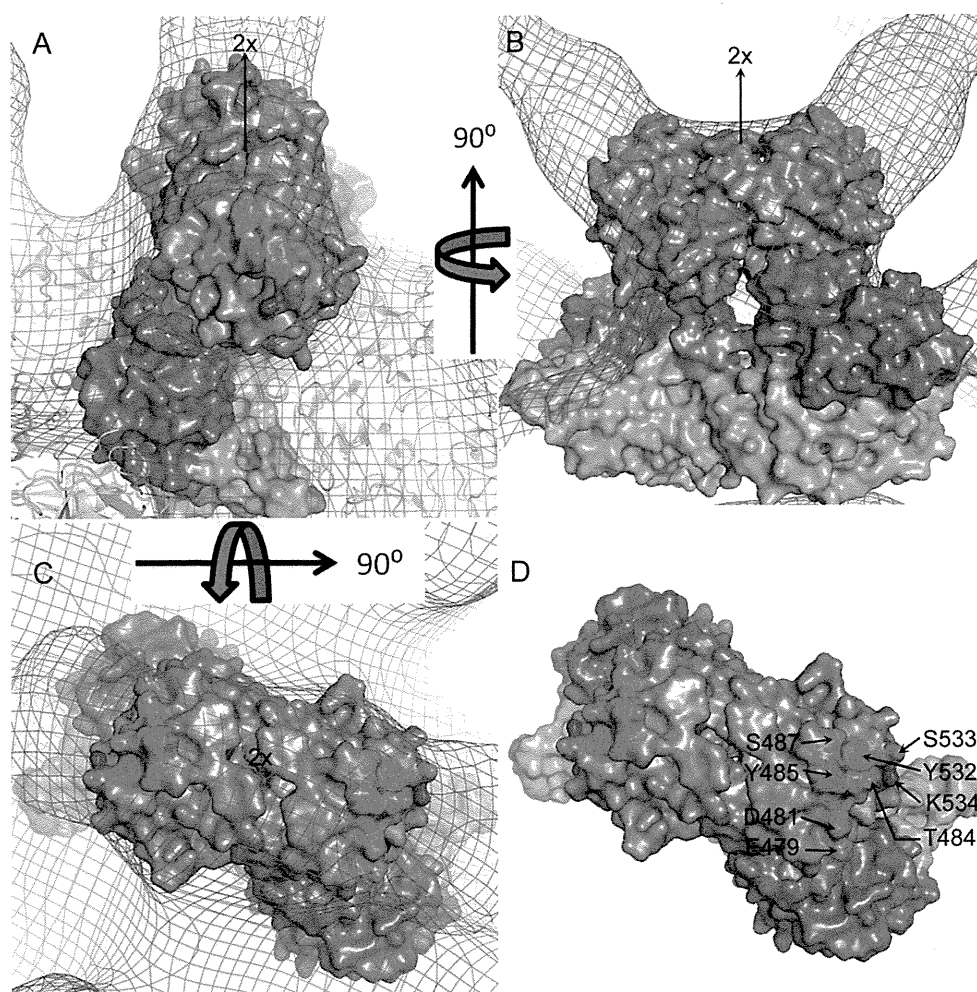
FIG. 3. The binding site of Fab224 antibody. (A) The cryo-EM density map of VLP-Fab224 was fitted with the crystal structure of PORF2 and viewed along a bound Fab molecule. One PORF2 dimer is presented as a solid surface and colored light magenta for the S domain, blue violet for the M domain, and dark gray for the P domain. The neighboring dimers are drawn in ribbon mode and colored wheat. (B) Side view of a PORF2 dimer fitted into the cryo-EM density map. (C) A PORF2 dimer viewed along the 2-fold axis and overlapped with the cryo-EM density map. (D) Top view of a PORF2 dimer viewed along the 2-fold axis. The amino acids in PORF2 responsible for binding to Fab224 are labeled. The PORF2 dimer is presented as a solid surface and colored in gray, violet, and light magenta for the P domain, the M domain, and the S domain, respectively. The residues along the Fab binding interface are colored according to the element, with green for carbon, blue for nitrogen, and red for oxygen.

side wall of the protruding domain toward the capsid shell, leaving its Fc domain exposed above the surface of the plateau (Fig. 2A). In contrast, the entire Fab224 molecule stood mainly on the top of the P domain surface. The Fab224 and the Fab4 molecules extend along the long axis of the P domain. In both cases, no steric hindrance of the Fab on the P domain with the neighboring Fab molecules at either the 5-fold or the 3-fold axes was apparent. The orientation of the Fabs relative to the plateau appeared different at a radius of 135 Å. The long axis of Fab224 tilted toward the neighboring spike, while the long axis of Fab4 pointed to the 5-fold axis (Fig. 2A).

To further analyze the Fab and HEV VLP binding interface, the crystal structure of genotype 1 PORF2 was docked onto the VLP-Fab224 cryo-EM density map. The genotype 1 PORF2 crystal structure (PDB ID 2ZZQ) is composed of three domains (31), and these domains are in good agreement with those of genotype 3 and genotype 4 PORF2 (PDB ID 2ZTN and 3HAG, respectively) (8, 32). The coordinates fitted very

well with the cryo-EM density map without any adjustment (CC value of 80%). The atoms on the surface of the HEV VLP capsid were plotted and colored according to their radial distance and overlapped with the density of the Fab at the surface plateau of the protruding spike (Fig. 2B).

The Fab224 interacted with the residues on the side of the ORF2 spike rather than with those residues on the spike's plateau surface (Fig. 3C). The contact footprint did not overlap with the dimeric interface of the PORF2 spike. As expected, Fab224 recognizes a conformational epitope, and its binding site covers a surface composed of three loops, including amino acids 470 to 493 in AB loop, amino acids 539 to 569 in CD loop, and amino acids 581 to 595 in EF loop (Fig. 3D). Residues E479, D481, T484, Y485, and S487 from the AB loop and residues Y532, S533, and K534 from the CD loop were in close contact with the Fab molecule.

Structure of HEV chimeric VLP. Chimeric HEV VLP-C-tag was constructed using a PORF2 fusion protein in which a
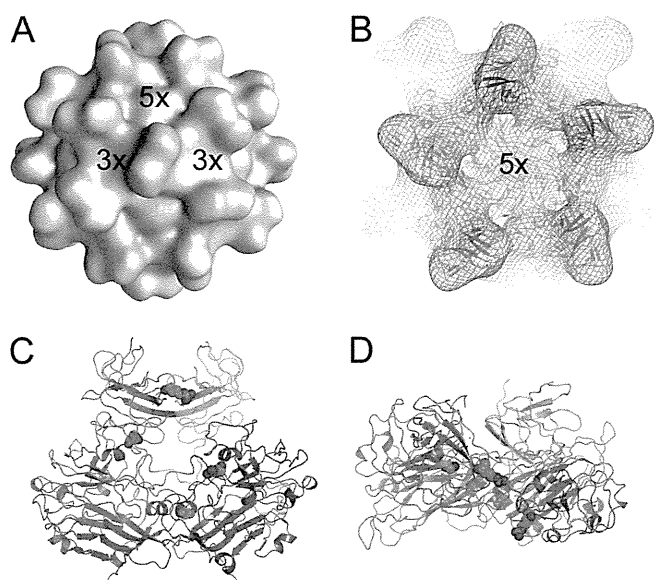
FIG. 4. The structure of the chimeric HEV VLP carrying a B-cell tag. (A) Surface presentation of VLP-C-tag viewed along an icosahedral 2-fold axis. (B) The cryo-EM density map of VLP-C-tag (mesh) was fitted with the crystal structure of the PORF2 decamer (ribbon). (C) Ribbon representation of PORF2 dimer with one monomer colored gray and the other colored pink for the S1 domain, blue for the M domain, and lime for the P domain. The amino acids prior to the four internal insertion sites are marked in sphere mode with color coding representing the elements as described in the Fig. 3 legend. (D) The top view of the PORF2 dimer, showing the location of the non-VLP insertion sites.

B-cell tag of 11 amino acids was incorporated into the C terminus of PORF2 (Fig. 1B). A total of 782 images of individual particles were used to reconstruct the final three-dimensional model of VLP-C-tag. In agreement with the previously published cryo-EM VLP structures, the surface of VLP-C-tag can

be divided into two distinct layers, an icosahedral shell and a protruding spike (Fig. 4A). The spike projects outward from the icosahedral shell and is composed of a PORF2 dimer. The distance between two adjacent spikes was ~76 Å as measured between the centers of the surface plateaus. These results are consistent with the measurements of VLPs obtained either from Tn5 insect cells (30) or from Sf9 insect cells (13), and no detectable density was added onto the outer surface of the spike. No RNA density was detected within the chimeric VLP-C-tag.

The crystal structure fit very well within the VLP-C-tag density map (Fig. 4B), indicating that the insertion of the C-terminal 11 amino acids inhibits neither the dimer-dimer interactions nor the formation of T=1 VLP. When the density maps were contoured to cover 100%, the radii of the S domains were roughly the same for both the VLP-C-tag and the VLP-Fab224 map, and the heights of the protruding spikes appeared similar. No density difference was observed from the docking (Fig. 5), suggesting that the inserted B-cell tag is flexible and less ordered. However, model fitting revealed that coordinates with unoccupied density appeared at the lateral side of the spike and underneath the Fab224 binding site (Fig. 5A and B), which may correspond to the inserted peptide.

DISCUSSION

HEV T=1 VLP is a vaccine candidate that induces protective immunity in nonhuman primates (12). It can also be used as an antigen carrier to deliver foreign epitopes through oral administration (20). Therefore, structural analysis of the antibody recognition sites is essential to suppress the neutralization effect of host vector-specific antibodies. For this purpose, we determined the structure of HEV VLP in complex with antibodies Fab224 (VLP-Fab224) and Fab4 (VLP-Fab4) and the structure of chimeric HEV VLP carrying a B-cell tag at the C terminus of PORF2 (VLP-C-tag). Docking the PORF2 crys-
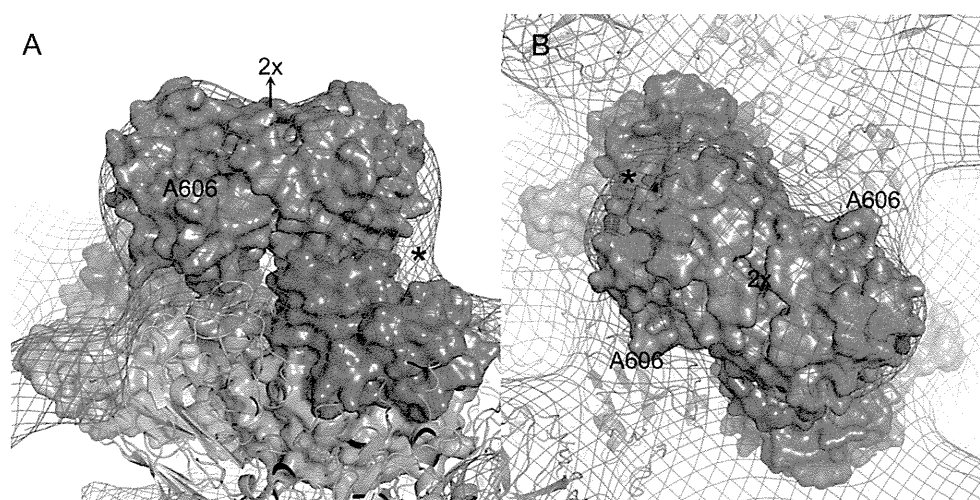

FIG. 5. Fitting of the PORF2 structure into the cryo-EM density map of HEV VLP-C-tag. The side view (A) and the top view (B) of the fitted PORF2 dimer (surface presentation) are overlapped with the cryo-EM density map of VLP-C-tag (mesh). The C-terminal residue A606 is located at the side of the protruding spike. One PORF2 dimer in the surface presentation is colored light magenta, blue violet, and gray for the S, M, and P domain, respectively. The ribbon representation shows the adjacent dimers. The amino acids in PORF2 responsible for binding to Fab224 are colored green for carbon, blue for nitrogen, and red for oxygen. Asterisks mark the location of the extra density that was not occupied with PORF2 coordinates.

tal structure provides spatial information on the HEV antigenic domain and structural guidance to better design foreign epitope insertion.

Structure of the neutralization epitopes. The antigenic properties of HEV and the mechanisms by which it is neutralized are difficult to characterize due to the lack of adequate cell culture replication systems. Therefore, our understanding of HEV immunology is mainly based on studies using recombinant proteins expressed in *E. coli* (23) and recombinant proteins or HEV VLPs generated using the baculovirus expression systems (15, 24). Data from these studies indicate that the C-terminal region of PORF2 participates in the immune response against HEV and that the HEV neutralization epitope is conformational. The minimum peptide required to induce HEV-neutralizing antibodies corresponds to a region of 148 residues in PORF2, from amino acids 459 to 607 (33). This peptide coincides with the P domain revealed in the crystal structures of PORF2. The density of the Fab in our cryo-EM structure interfaced entirely with the spikes, thus confirming that the P domain is primarily responsible for HEV antigenicity. Fab4 is a chimpanzee antibody that recognizes the ORF2 protein and was isolated from a cDNA library by using phage display (25). Fab4 binds to native HEV virions and recombinant PORF2 peptides containing amino acids 597 to 607 (26). We performed fitting with the VLP-Fab4 structure; however, the Fab4 density was too weak to conclusively determine the Fab4 binding site on the surface of HEV VLP. However, the density corresponding to the Fab4 molecule did cover amino acid 606 (data not shown). It is not clear why Fab224 appeared not to interact with peptides lacking amino acids 599 to 608 in immunoblot analysis. However, the Fab224 binding site is consistent with the critical antigenic residues determined previously using mutagenesis. It was found that double mutations that changed residues E479 and K534 or Y485 and I529 to alanine selectively abrogated PORF2's reactivity with neutralizing antibodies (11). Experiments with another set of mutants defined the same region as the HEV antigenic domain, with antibody recognition residues spreading over the AB, CD, and EF loops (32). The antibodies used in both experiments were neutralizing antibodies; therefore, the Fab224 binding surface is part of the dominant neutralization site, suggesting that the monoclonal antibody Fab224 is a neutralizing antibody. This neutralization site partially overlaps with the receptor binding site (32), and antibody binding may create spatial hindrance that prevents HEV VLPs from attaching to the cell surface.

Insertion sites for foreign epitopes. Because they are highly organized capsids that mimic the overall structure of virus particles, VLPs are a robust means by which to simultaneously carry small molecules, peptide antigenic epitopes, and DNA vaccines from heterogeneous sources to target disease sites. However, this rational vaccine design relies on excellent VLP structural information so that epitopes can be effectively conjugated to the VLP surface. In a previous study, rather than selecting PORF2 insertion sites on the basis of structural information, six insertion sites were selected according to restriction enzyme sites located either internally (four sites) or in the N or C terminus of PORF2. The internal sites are located after residues A179, R366, A507, and R542. Fusion proteins carrying insertions at sites A179 and R336 completely failed to produce VLPs, and insertions at A507 and R542 greatly re-

duced VLP production (20). Crystal structure data revealed that the spatial position of these sites is disadvantageous. Residue A179 is located in the S domain in the middle of an α-helix, which is necessary for the integrity of the S domain and its interaction with the 2-fold-related neighboring subunit. R366 is located in the M domain and favors electrostatic interaction with residue E386 from the 3-fold-related neighboring subunit. Although located within the P domain, the side chain of R542 is within the dimeric interface and guides the hydrophobic interaction of the two monomers. Replacement of R542 may misalign the orientation between two P domains and weaken the dimeric interaction between PORF2 proteins. Residue A507 in the P domain plays an important role in maintaining P domain orientation by fixing the angle of the long proline-rich hinge. Moreover, none of the four residues are exposed on the surface of VLPs, although some of them are located on the surface of individual PORF2 subunits (Fig. 4C and D). Therefore, the insertion of a foreign sequence at these sites does not interfere with the expression of individual proteins but, rather, hinders the assembly of HEV VLPs. The crystal structure revealed that the C terminus is exposed on the surface of VLPs, while the N terminus points toward the VLP center. Therefore, insertion at these two sites does not inhibit VLP assembly; however, the C terminus is more suitable for tethering bulky foreign antigenic sequences, as was shown in a previous report (20).

The cryo-EM structure of the chimeric HEV VLP-C-tag suggested that the B-cell tag was located at the lateral side of the spike, not far from residue A606 (C-terminal end in the crystal structure) (Fig. 5A). This density is located beneath the Fab224 binding site but nonetheless overlaps with the potential binding site of Fab4. As a result, the insertion of the 11-amino-acid B-cell sequence may leave the HEV antigenic site partially open and accessible to the host immune system. This explains why mice can develop antibodies against both HEV and the foreign epitope after oral administration of VLP-C-tag (20).

In conclusion, the cryo-EM structures of VLP-Fab224 identified the lateral surface of the P domain as the recognition site for anti-HEV neutralizing antibodies. The insertion of a B-cell epitope at the PORF2 C terminus does not interfere with T=1 VLP assembly. Thus, T=1 HEV VLPs are a novel tool for oral vaccine delivery, as they constitute nonreplicating entities that can induce mucosal immunity without adjuvant. The induction of antibodies against both HEV and the target disease is an additional advantage of this delivery system.

REFERENCES

1. **Adler, B., and S. Faine.** 1983. A pomona serogroup-specific, agglutinating antigen in Leptospira, identified by monoclonal antibodies. Pathology **15:** 247–250.

2. **Baker, T., and H. Cheng.** 1996. A model based approach for determining orientations of biological macromolecules imaged by cryo-electron microscopy. J. Struct. Biol. **116:**120–130.

3. **Bendall, R. P., V. Ellis, S. Ijaz, P. Thurairajah, and H. R. Dalton.** 2008. Serological response to hepatitis E virus genotype 3 infection: IgG quantitation, avidity, and IgM response. J. Med. Virol. **80:**95–101.

4. **Crowther, R. A.** 1971. Procedures for three-dimensional reconstruction of spherical viruses by Fourier synthesis from electron micrographs. Philos. Trans. R. Soc. Lond. B Biol. Sci. **261:**221–230.

5. **DeLano, W. L.** 2002. The PYMOL molecular graphics system. DeLano Scientific, Palo Alto, CA.

6. **Deshmukh, T. M., K. S. Lole, A. S. Tripathy, and V. A. Arankalle.** 2007. Immunogenicity of candidate hepatitis E virus DNA vaccine expressing complete and truncated ORF2 in mice. Vaccine **25:**4350–4360.

7. **Emerson, S., P. Clemente-Casares, N. Moiduddin, V. A. Arankalle, U. Torian, and R. Purcell.** 2006. Putative neutralization epitopes and broad cross-genotype neutralization of hepatitis E virus confirmed by a quantitative cell-culture assay. J. Gen. Virol. **87:**697–704.

8. **Guu, T., Z. Liu, Q. Ye, D. Mata, K. Li, C. Yin, J. Zhang, and Y. Tao.** 2009. Structure of the hepatitis E virus-like particle suggests mechanisms for virus assembly and receptor binding. Proc. Natl. Acad. Sci. U. S. A. **106:**12992–12997.

9. **Jones, T. A., J. Y. Zou, S. W. Cowan, and M. Kjeldgaard.** 1991. Improved method for building protein models in electron density maps and the location of errors in these models. Acta Crystallogr. A **47**(Pt. 2)**:**110–119.

10. **Khuroo, M. S., and M. S. Khuroo.** 2008. Hepatitis E virus. Curr. Opin. Infect. Dis. **21:**539–543.

11. **Li, S., S. Tang, J. Seetharaman, C. Y. Yang, Y. Gu, J. Zhang, H. Du, J. W. Shih, C. L. Hew, J. Sivaraman, and N. S. Xia.** 2009. Dimerization of hepatitis E virus capsid protein E2s domain is essential for virus-host interaction. PLoS Pathog. **5:**e1000537.

12. **Li, T.-C., Y. Suzaki, Y. Ami, T. N. Dhole, T. Miyamura, and N. Takeda.** 2004. Protection of cynomolgus monkeys against HEV infection by oral administration of recombinant hepatitis E virus-like particles. Vaccine **22:**370–377.

13. **Li, T.-C., N. Takeda, T. Miyamura, Y. Matsuura, J. C. Y. Wang, H. Engvall, L. Hammar, L. Xing, and R. H. Cheng.** 2005. Essential elements of the capsid protein for self-assembly into empty virus-like particles of hepatitis E virus. J. Virol. **79:**12999–13006.

14. **Li, T., N. Takeda, and T. Miyamura.** 2001. Oral administration of hepatitis E virus-like particles induces a systemic and mucosal immune response in mice. Vaccine **19:**3476–3484.

15. **Li, T. C., Y. Yamakawa, K. Suzuki, M. Tatsumi, M. A. Razak, T. Uchida, N. Takeda, and T. Miyamura.** 1997. Expression and self-assembly of empty virus-like particles of hepatitis E virus. J. Virol. **71:**7207–7213.

16. **Maloney, B. J., N. Takeda, Y. Suzaki, Y. Ami, T. C. Li, T. Miyamura, C. J. Arntzen, and H. S. Mason.** 2005. Challenges in creating a vaccine to prevent hepatitis E. Vaccine **23:**1870–1874.

17. **Minuk, G. Y., A. Sun, D. F. Sun, J. Uhanova, L. E. Nicolle, B. Larke, and A. Giulivi.** 2007. Serological evidence of hepatitis E virus infection in an indigenous North American population. Can. J. Gastroenterol. **21:**439–442.

18. **Mushahwar, I. K.** 2008. Hepatitis E virus: molecular virology, clinical features, diagnosis, transmission, epidemiology, and prevention. J. Med. Virol. **80:**646–658.

19. **Naik, S. R., R. Aggarwal, P. N. Salunke, and N. N. Mehrotra.** 1992. A large waterborne viral hepatitis E epidemic in Kanpur, India. Bull. World Health Organ. **70:**597–604.

20. **Niikura, M., S. Takamura, G. Kim, S. Kawai, M. Saijo, S. Morikawa, I. Kurane, T. C. Li, N. Takeda, and Y. Yasutomi.** 2002. Chimeric recombinant hepatitis E virus-like particles as an oral vaccine vehicle presenting foreign epitopes. Virology **293:**273–280.

21. **Pavio, N., and J. M. Mansuy.** 2010. Hepatitis E in high-income countries. Curr. Opin. Infect. Dis. **23:**521–527.

22. **Pettersen, E. F., T. D. Goddard, C. C. Huang, G. S. Couch, D. M. Greenblatt, E. C. Meng, and T. E. Ferrin.** 2004. UCSF Chimera—a visualization system for exploratory research and analysis. J. Comput. Chem. **25:**1605–1612.

23. **Riddell, M. A., F. Li, and D. A. Anderson.** 2000. Identification of immunodominant and conformational epitopes in the capsid protein of hepatitis E virus by using monoclonal antibodies. J. Virol. **74:**8011–8017.

24. **Robinson, R. A., W. H. Burgess, S. U. Emerson, R. S. Leibowitz, S. A. Sosnovtseva, S. Tsarev, and R. H. Purcell.** 1998. Structural characterization of recombinant hepatitis E virus ORF2 proteins in baculovirus-infected insect cells. Protein Expr. Purif. **12:**75–84.

25. **Schofield, D. J., J. Glamann, S. U. Emerson, and R. H. Purcell.** 2000. Identification by phage display and characterization of two neutralizing chimpanzee monoclonal antibodies to the hepatitis E virus capsid protein. J. Virol. **74:**5548–5555.

26. **Schofield, D. J., R. H. Purcell, H. T. Nguyen, and S. U. Emerson.** 2003. Monoclonal antibodies that neutralize HEV recognize an antigenic site at the carboxyterminus of an ORF2 protein vaccine. Vaccine **22:**257–267.

27. **Tsarev, S. A., T. S. Tsareva, S. U. Emerson, S. Govindarajan, M. Shapiro, J. L. Gerin, and R. H. Purcell.** 1997. Recombinant vaccine against hepatitis E: dose response and protection against heterologous challenge. Vaccine **15:**1834–1838.

28. **Worm, H. C., and G. Wirnsberger.** 2004. Hepatitis E vaccines: progress and prospects. Drugs **64:**1517–1531.

29. **Xiao, C., and M. G. Rossmann.** 2007. Interpretation of electron density with stereographic roadmap projections. J. Struct. Biol. **158:**181–186.

30. **Xing, L., K. Kato, T. Li, N. Takeda, T. Miyamura, L. Hammar, and R. H. Cheng.** 1999. Recombinant hepatitis E capsid protein self-assembles into a dual-domain T=1 particle presenting native virus epitopes. Virology **265:**35–45.

31. **Xing, L., T. C. Li, N. Miyazaki, M. N. Simon, J. S. Wall, M. Moore, C. Y. Wang, N. Takeda, T. Wakita, T. Miyamura, and R. H. Cheng.** 2010. Structure of hepatitis E virion-sized particle reveals an RNA-dependent viral assembly pathway. J. Biol. Chem. **285:**33175–33183.

32. **Yamashita, T., Y. Mori, N. Miyazaki, H. Cheng, M. Yoshimura, H. Unno, R. Shima, K. Moriishi, T. Tsukihara, T. C. Li, N. Takeda, T. Miyamura, and Y. Matsuura.** 2009. Biological and immunological characteristics of hepatitis E virus-like particles based on the crystal structure. Proc. Natl. Acad. Sci. U. S. A. **106:**12986–12991.

33. **Zhou, Y. H., R. Purcell, and S. Emerson.** 2005. A truncated ORF2 protein contains the most immunogenic site on ORF2: antibody responses to nonvaccine sequences following challenge of vaccinated and nonvaccinated macaques with hepatitis E virus. Vaccine **23:**3157–3165.

Acquisition of HIV-1 Resistance in T Lymphocytes Using an ACA-Specific *E. coli* mRNA Interferase

Hideto Chono,[1,2] Kazuya Matsumoto,[1] Hiroshi Tsuda,[1,2] Naoki Saito,[1,2] Karim Lee,[3]
Sujeong Kim,[4] Hiroaki Shibata,[5] Naohide Ageyama,[5] Keiji Terao,[5] Yasuhiro Yasutomi,[5]
Junichi Mineno,[1] Sunyoung Kim,[3] Masayori Inouye,[6] and Ikunoshin Kato[1,2]

Abstract

Transcriptional activation of gene expression directed by the long terminal repeat (LTR) of HIV-1 requires both the transactivation response element (TAR) and Tat protein. HIV-1 mutants lacking a functional *tat* gene are not able to proliferate. Here we take a genetic approach to suppress HIV-1 replication based on Tat-dependent production of MazF, an ACA-specific endoribonuclease (mRNA interferase) from *Escherichia coli*. When induced, MazF is known to cause Bak- and NBK-dependent apoptotic cell death in mammalian cells. We first constructed a retroviral vector, in which the *mazF* (ACA-less) gene was inserted under the control of the HIV-1 LTR, which was then transduced into CD4+ T-lymphoid CEM-SS cells in such a way that, upon HIV-1 infection, the *mazF* gene is induced to destroy the infecting HIV-1 mRNA, preventing HIV-1 replication. Indeed, when the transduced cells were infected with HIV-1 IIIB, the viral replication was effectively inhibited, as HIV-1 IIIB p24 could not be detected in the culture medium. Consistently, not only cell growth but also the CD4 level was not affected by the infection. These results suggest that the HIV-1-LTR-regulated *mazF* gene was effectively induced upon HIV-1 IIIB infection, which is sufficient enough to destroy the viral mRNA from the infected HIV-1 IIIB to completely block viral proliferation in the cells, but not to affect normal cell growth. These results indicate that the T cells transduced with the HIV-1-LTR-regulated *mazF* gene acquire HIV-1 resistance, providing an intriguing potential for the use of the HIV-1-LTR-regulated *mazF* gene in anti-HIV gene therapy.

Introduction

RNASE-BASED STRATEGIES for anti-human immunodeficiency virus (HIV) gene therapy may be superior to RNA-based (antisense, ribozyme, or siRNAs) strategies, because the former strategies evade the effects of frequent resistant mutations in HIV-1. MazF is a unique sequence-specific endoribonuclease, or mRNA interferase, encoded by the *Escherichia coli* genome (Zhang *et al.*, 2003). It cleaves mRNA at ACA-specific sequences and effectively inhibits protein synthesis. To date, a number of MazF homologues have been found in various bacteria. These homologues have a wide range of sequence specificities and cleave three- to five-nucleotide RNA sequences in transcripts that play diverse roles in bacterial physiology (Zhu *et al.*, 2006, Yamaguchi and Inouye, 2009), including cell-growth regulation, specific gene

regulation (Zhu *et al.*, 2009), and obligatory programmed cell death (Nariya and Inouye, 2008). Induction of *E. coli* MazF mRNA interferase in mammalian cells has been demonstrated to effectively induce Bak- and NBK-dependent apoptotic cell death (Shimazu *et al.*, 2007), indicating that MazF mRNA interferase may be a new and effective tool for gene therapy.

In the HIV-1 life cycle immediately after HIV-1 infection, Tat (transactivator of transcription), an early regulatory protein encoded by the HIV-1 genome, is produced, which subsequently binds to the TAR (transactivation response) sequence to induce the transcription of the HIV-1 genome leading to the expression of other HIV-1 proteins (Berkhout *et al.*, 1989). Therefore, for prevention of HIV-1 infection, it would be a best strategy to preferentially destroy the HIV-1 transcript upon HIV-1 infection. For this purpose, we constructed a Tat-dependent MazF expression system in a

[1]Center for Cell and Gene Therapy, Takara Bio Inc., Otsu, Shiga, 520-2193, Japan.
[2]Biotechnology Research Laboratories, Takara Bio Inc., Otsu, Shiga, 520-2193, Japan.
[3]Department of Biological Sciences, Seoul National University, Seoul 151-742, Korea.
[4]ViroMed Co. Ltd., Seoul 151-818, Korea.
[5]Tsukuba Primate Research Center, National Institute of Biomedical Innovation, Tsukuba, Ibaraki, 305-0843, Japan.
[6]Department of Biochemistry, Robert Wood Johnson Medical School, Piscataway, NJ 08854, USA.

35

retroviral vector, in which the *mazF* gene was fused downstream of the TAR sequence. As the *E. coli mazF* open-reading frame contains nine ACA sequences, all of them were engineered to MazF-uncleavable sequences without changing the amino acid sequence of MazF. This vector was then transduced into T cells so that MazF production is expected to be induced upon HIV-1 infection. Note that Tat protein produced upon HIV-1 infection induces not only the transcription of infected HIV-1, but also the transcription of the HIV-1 long terminal repeat (LTR)-regulated *mazF* (ACA-less) gene integrated into the genome of the T cells. In the present article, CD4+ T lymphoid line CEM-SS cells were used as T cells, which were transduced with the retroviral vector containing the Tat-inducible *mazF* (ACA-less) gene under the HIV-1-LTR promoter. When the transduced cells were infected with HIV-1 IIIB, the replication of the infected virus was effectively inhibited without affecting cell growth. Notably, the CD4 level after HIV-1 IIIB infection was not affected either. These results suggest that the HIV-1-LTR-regulated *mazF* (ACA-less) gene was effectively induced upon HIV-1 IIIB infection, which is sufficient enough to destroy the viral mRNA from the infected HIV-1 IIIB to completely block viral proliferation in the cells. However, the level of MazF induced is not enough to cause any serious cellular damage, thus maintaining normal cell growth and the CD4 level. These results suggest an intriguing potential for the use of the HIV-1-LTR-regulated *mazF* (ACA-less) gene in anti-HIV gene therapy.

Materials and Methods

Cell lines

293T (ATCC no. CRL-11268) cells were cultured in Dulbecco's modified Eagle medium (DMEM; Sigma-Aldrich, Steinheim, Germany) supplemented with 10% (v/v) fetal bovine serum (FBS; Invitrogen, Carlsbad, CA). CEM-SS cells (Kim *et al.*, 1989) were cultured in RPMI-1640 (Sigma-Aldrich) containing 10% (v/v) FBS (Invitrogen). The doubling time of the cells for each culture condition was calculated by linear regression analysis using Microsoft Excel software (Microsoft, Seattle, WA).

Retroviral vectors

The self-inactivating retroviral vector pMTD3 was constructed by deleting a segment consisting of 267 nucleotides from the 3'LTR U3 region of pMT (Lee *et al.*, 2004). An ACA-less *mazF* gene was synthesized by engineering all nine ACA sequences in the original *E. coli mazF* gene to MazF-uncleavable sequences without changing the amino acid sequence of MazF. The HIV-LTR fragment was obtained from pQBI-LTRgagGFP (Quantum Biotechnologies Inc., Montreal, QC, Canada). To minimize the HIV-LTR sequence, U3-TAR fragments were obtained by PCR. The ACA-less *mazF* gene was inserted downstream of U3-TAR to obtain the final self-inactivating retroviral vector plasmid, pMTD3-U3TAR-MazF. As a control, the green fluorescent protein (GFP) gene was inserted into the vector to obtain pMTD3-U3TAR-GFP.

To mimic HIV replication, two kinds of retroviral vectors that express the HIV-1 Tat protein were constructed as follows: (1) Constitutitve Tat expression system from MLV-LTR. The HIV-1 *tat* gene was synthesized and inserted

at the multiple-cloning site of pMT. To easily monitor the gene expression in transduced cells, an internal ribosome entry site (IRES) and a coding region for a fluorescent protein, ZsGreen, were fused downstream of the *tat* gene. Thus, the resulting plasmid, pM-LTR-Tat-ZG, expresses Tat as well as ZsGreen from MLV-LTR. (2) Tat expression system from the HIV-1 LTR. The HIV-LTR-*tat*-polyA cassette was inserted in the opposite direction of pMT, and the ZsGreen marker gene was expressed from a phosphoglycerate kinase (PGK) promoter in the normal orientation of pMT. The resulting vector plasmid was designated as pH-LTR-Tat-ZG.

To enhance the viral titer for efficient *mazF* gene transduction, the HIV-LTR-MazF-polyA cassette was introduced in the opposite direction of the MoMLV-LTR at the multicloning site of pMT plasmid (Lee *et al.*, 2004). A truncated form of the human low-affinity nerve growth factor gene (ΔLNGFR) (Verzeletti *et al.*, 1998) was also introduced into the retrovirus vector as a surface marker. The ΔLNGFR gene is under the control of human PGK promoter. The resultant vector plasmid was designated as pMT-MFR-PL2 (Fig. 1B).

Preparation of retroviral vectors

The self-inactivating retroviral vector was generated by the transient transfection method as follows: The GALV-*env* expression vector plasmid, pVM-GeR, was constructed by replacing the amphotropic-*env* gene of pVM-AE (Yu *et al.*, 2003) with the gibbon ape leukemia virus envelope gene. The GALV-env retroviral vector was produced by co-transfecting 293T cells with the retroviral *gag-pol* expression vector plasmid, pVM-GP (Yu *et al.*, 2003), pVM-GeR, and the self-inactivating retroviral vector plasmid. Two days after transfection, viral supernatant was harvested by filtration of the culture fluid from 293T cells with use of a 0.45-μm filter.

GALV-enveloped retroviral Tat expression vectors and MazF expression vector were also generated as follows: Ecotropic retroviral vectors were generated by the transient transfection method using the packaging plasmids pGP (MLV-*gag-pol*; Takara Bio, Otsu, Shiga, Japan) and pE-eco (ecotropic *env*; Takara Bio) with the retroviral vector plasmid pM-LTR-Tat-ZG, pH-LTR-Tat-ZG, or pMT-MFR-PL2. This was performed with use of human embryonic kidney 293T-derived G3T-hi cells (Takara Bio) by using the calcium phosphate co-transfection method. The GALV-*env* retroviral vector was obtained from PG13 packaging cells (ATCC no. CRL-10686) by infection with the ecotropic retrovirus vector as prepared above. After selection of the infected PG13 cells, the virus was collected from the growth medium by filtration of the supernatant with use of a low-protein binding filter (0.45 μm).

Retroviral transduction into CEM-SS cells

CEM-SS cells were infected with self-inactivating retroviral vectors in the presence of 8 μg/ml Polybrene (hexadimethrine bromide; Sigma-Aldrich). Polyclonal gene-transduced cell populations were obtained by selecting the cells with G418 (Invitrogen) at a concentration of 1 mg/ml.

CEM-SS cells or CEM-SS cells transduced with MTD3-U3TAR-MazF were infected with Tat expression retroviral vectors M-LTR-Tat-ZG or H-LTR-Tat-ZG in the presence of RetroNectin (Takara Bio) according to the manufacturer's protocol.

FIG. 1. Construction of retroviral vector under the control of HIV-LTR promoter. To remove promoter activity of the MoMLV LTR, the self-inactivating retroviral vector pMTD3 was constructed based on pMT (Lee *et al.*, 2004) by deleting a 276-bp fragment from its 3'LTR U3 region. A synthetic ACA-less *mazF* gene was then inserted downstream of HIV-1 U3-TAR resulting in the self-inactivating retroviral vector, pMTD3-U3TAR-MazF. As a control, the GFP gene was inserted in place of the *mazF* gene, which resulted in pMTD3-U3TAR-GFP. The self-inactivating retroviral vectors were generated using the transient transfection method with the packaging plasmids MoMLV-gag-pol, GALV-env,

and the self-inactivating retroviral vector in 293T cells. The viral preparation was obtained 2 days after transfection by filtering the culture supernatant. To improve the viral titer for efficient gene transduction over an initial vector, HIV-LTR-MazF-polyA cassette was inserted in the opposite direction of the MoMLV-LTR at the multi-cloning site of pMT. A truncated form of the human low-affinity nerve growth factor gene (ΔLNGFR) (Verzeletti *et al.*, 1998) was used as a surface marker. The resultant vector plasmid was designated pMT-MFR-PL2. GALV-env retroviral vector was generated as described in Materials and Methods.
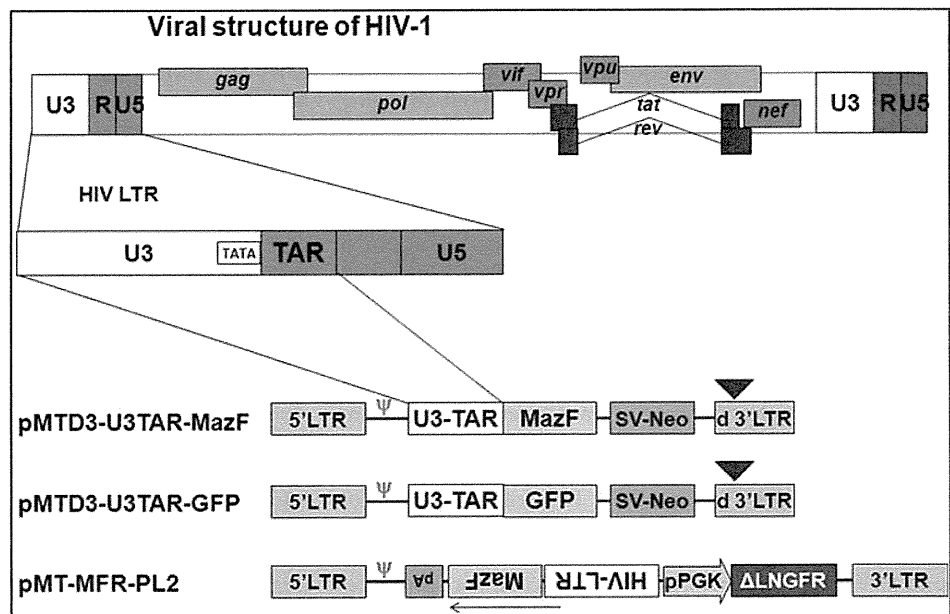
Retroviral transduction into primary rhesus macaque CD4+ T cells

Rhesus macaque CD4+ T cells were isolated from peripheral blood mononuclear cells (PBMC) using anti-CD4 monoclonal antibody-conjugated beads (Dynal CD4 Positive Isolation Kit; Invitrogen). Prior to gene transduction, the isolated CD4+ T cells were activated for 3 days with a combination of anti-monkey-CD3 clone FN-18 (BioSource, Camarillo, CA) and anti-human-CD28 monoclonal antibody clone L293 (BD Biosciences, Franklin Lakes, NJ)-conjugated beads at a cell-to-bead ratio of 1:1 in GT-T503 (Takara Bio) supplemented with 10% FBS and 200 IU of interleukin-2 (Chiron, Emeryville, CA). On day 3, activated CD4+ T cells were infected with the MazF retroviral vector (MT-MFR-PL2) in the presence of RetroNectin (Takara Bio) as per the manufacturer's instructions. The transduction was repeated again on day 4. The cells were further incubated for another 3 days. The genetically modified cells marked with the ΔLNGFR+ were concentrated with anti-CD271 monoclonal antibody-conjugated beads (CD271 MicroBeads; Miltenyi Biotec, Bergisch Gladbach, Germany). Aliquots of the *mazF* gene-modified cells (designated as MazF-Tmac cells) were collected and cryopreserved until use. As a control, the nontransduced CD4+ T cells were also prepared using the same method as used above.

HIV infection

CEM-SS cells and CEM-SS cells transduced with MTD3-U3TAR-MazF or MTD3-U3TAR-GFP were infected with HIV-1 IIIB at the different multiplicities of infection (MOIs) of 0.07, 0.0007, and 0.00007. After infection, cells were washed with PBS and subsequently cultured in 10 ml of RPMI

1640 containing 10% FBS. HIV-1 p24 levels in the culture supernatant were calculated using the p24 ELISA kit (PerkinElmer, Waltham, MA). Viable cell numbers were measured using the trypan blue exclusion assay. The doubling time of cells was calculated by logistic regression analysis of each growth curve for the HIV-1 infection sets.

SHIV infection

The cryopreserved cells of the control CD4+ T and MazF-Tmac cells were recovered in GT-T503 medium supplemented with 10% FBS and 200 IU of interleukin-2 and reactivated with anti-monkey-CD3 and anti-human-CD28 monoclonal antibody-conjugated beads at a cell-to-bead ratio of 5:1. After a 6-day incubation, the cells were infected with simian/human immunodeficiency virus (SHIV) 89.6P (Reimann *et al.*, 1996) at the MOI of 0.01 and cultured for 6 more days. SHIV RNA levels in the culture supernatant and intracellular RNAs were determined by using quantitative real-time PCR (Thermal Cycler Dice Real Time System; Takara Bio Inc.) with a set of specific primers designed in the SHIV *gag* region (Miyake *et al.*, 2006).

Flow cytometry

Flow cytometry was used for the analysis of surface CD4 expression and transduction efficiency. Endogenous expression levels of CD4 in CEM-SS cells and CEM-SS cells transduced with MTD3-U3TAR-MazF were analyzed using phycoerythrin (PE)-labeled anti-human CD4 antibody (Beckman Coulter, Fullerton, CA). Intracellular p24 levels were analyzed using fluorescein isothiocyanate-labeled anti-p24 antibody (Beckman Coulter) after the cells were fixed and permeabilized for flow cytometric analysis.

Gene transfer efficiencies of the retroviral Tat expression vector into CEM-SS cells and CEM-SS cells transduced with MTD3-U3TAR-MazF were analyzed by detecting the ZsGreen marker fluorescence. Immediately before flow cytometry, propidium iodide (PI) was added at the concentration of 100 ng/ml to stain dead cells. Samples were run through a FACSCantoII flow cytometer (BD Biosciences), and data were analyzed using the FACSDiva software (BD Biosciences).

Genomic DNA analysis

Genomic DNA was extracted by phenol/chloroform extraction from CEM-SS cells and CEM-SS cells transduced with MTD3-U3TAR-MazF cells infected with HIV-1 IIIB at

the MOI of 0.007. Two different regions of the HIV-1 *gag* gene (246–467 and 905–1046) were amplified by PCR at 14 days after HIV-1 IIIB infection. As a positive control, genomic DNA was amplified from H9 cells chronically infected with HIV-1 IIIB. Human mitochondrial DNA (mtDNA) was amplified as a control for the PCR.

Co-culture with chronically infected cells

The CEM-SS cell line chronically infected with HIV-1 IIIB (CH-1) was mixed with CEM-SS cells or CEM-SS cells transduced with MTD3-U3TAR-MazF. CH-1 cells were mixed at different ratios of 10, 1, or 0.1%. After 6 and 14 days of infection, intracellular p24 levels were analyzed by flow cytometric analyses.
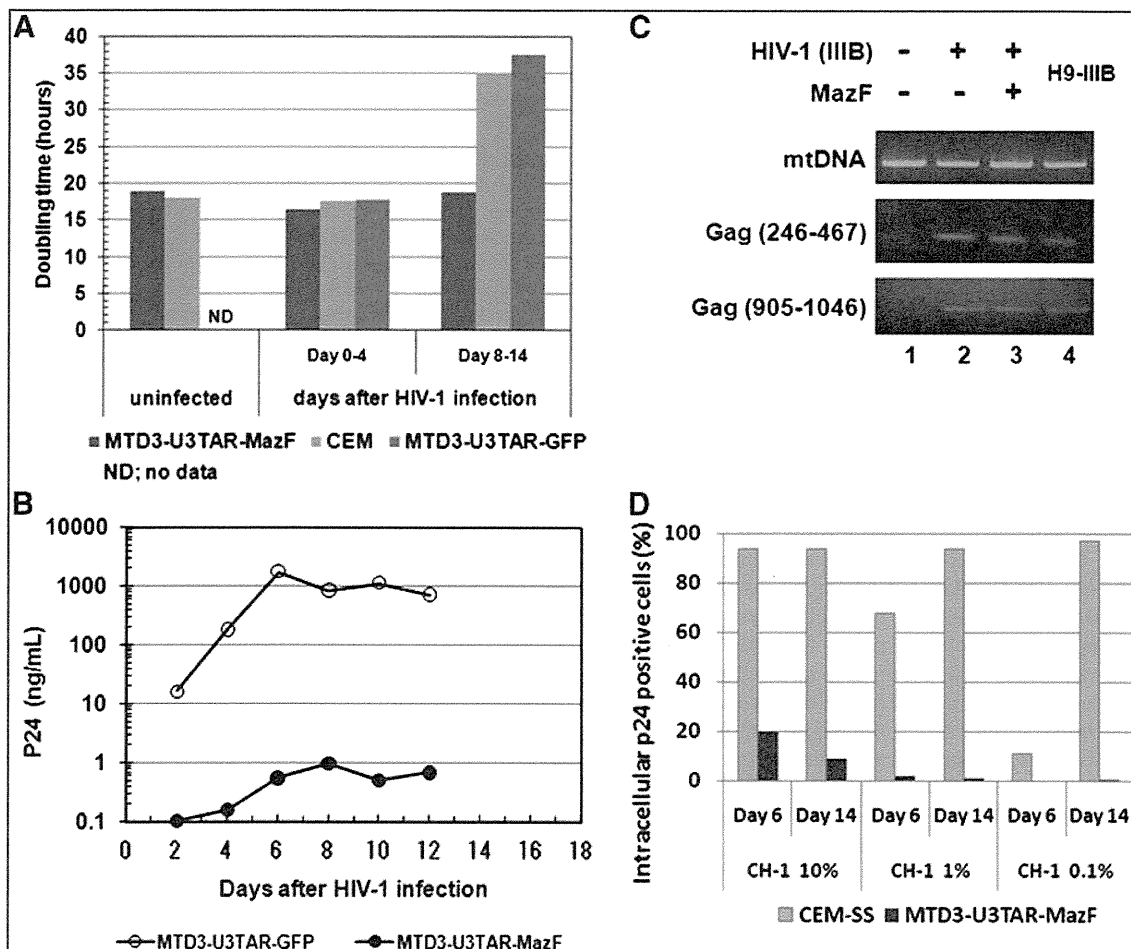

FIG. 2. Analysis of MazF-transduced CEM-SS cells after HIV-1 infection. (A) CEM-SS cells transduced with either the *mazF* gene or the GFP gene were infected with HIV-1 IIIB at an MOI of 0.07. After infection, the doubling time of the cells for each culture condition was calculated using linear regression analysis using Microsoft Excel software. The square of the correlation coefficient (R^2) between culture day and log (cell number) values was observed to be >0.97. (B) HIV-1 p24 levels in the culture supernatant were estimated using the p24 ELISA kit. Filled circles indicate p24 levels in the supernatant of CEM-SS cells transduced with MTD3-U3TAR-MazF. Open circles indicate p24 levels in the supernatant of CEM-SS cells transduced with MTD3-U3TAR-GFP. (C) Genomic DNA PCR analysis of CEM-SS cells and MazF-transduced CEM-SS cells infected with HIV-1 IIIB at an MOI of 0.007. Two different regions of the HIV-1 *gag* gene (246–467 and 905–1046) were amplified by PCR at 14 days after HIV-1 IIIB infection. As a positive control, the genomic DNA was amplified from H9 cells chronically infected with HIV-1 IIIB. Human mtDNA was amplified as a control for the PCR reaction. (D) Intracellular p24 levels were analyzed in the mixtures of CEM-SS cell lines chronically infected with HIV-1 IIIB (CH-1) using CEM-SS cells or MazF-transduced CEM-SS cells. CH-1 cells were mixed at different ratios of 10, 1, or 0.1%. After 6 and 14 days of infection, cells were stained with an anti-HIV-1 p24 antibody and subjected to flow cytometric analysis.

Results

We first constructed the retroviral vector system in which the gene for MazF was inserted downstream of the HIV-1 TAR sequence (Fig. 1). As the *E. coli mazF* gene contains nine ACA sequences in its open-reading frame, all of these ACA sequences were first engineered to other MazF-uncleavable sequences without altering the amino acid sequence of MazF to make the *mazF* mRNA resistant to MazF. The resulting self-inactivating retroviral vector (MTD3-U3TAR-MazF) was used to transduce CD4+ T lymphoid CEM-SS cells to create a system in which MazF induction in CEM-SS cells upon infection with HIV-1 effectively suppressed HIV-1 replication without causing apoptosis of infected T cells. The MTD3 retroviral vector contained an intact 5′ LTR and a mutated 3′ LTR that lacks most of the transcriptional elements present in U3. Cells transduced with the resulting retroviral vector contained the defective LTR at both ends (Yu *et al.*, 1986). The self-inactivating retroviral vector was transiently produced and subsequently transduced into the human T lymphoid line CEM-SS cells, which are highly susceptible to HIV infection. Transduced cells were subjected to G418 selection to obtain drug-resistant populations. A GFP-expressing retroviral vector under the control of HIV-LTR (MTD3-U3TAR-GFP) was also used as a control.

The growth rate of CEM-SS cells transduced with MTD3-U3TAR-MazF was comparable to that of the parental CEM-SS line (Fig. 2A), suggesting that MazF expression was tightly controlled and did not inhibit cell growth. Furthermore, the CD4 levels of MTD3-U3TAR-MazF-transduced CEM-SS cells were identical to those of the parental CEM-SS cells (Fig. 3A).

To investigate the effects of HIV-1 infection, MazF-transduced or GFP-transduced CEM-SS cells were infected with HIV-1 IIIB at different MOIs, specifically 0.07, 0.0007, and 0.00007 (Fig. 4). Levels of the HIV-1 p24 antigen in the culture media were examined 16 days post infection. As shown in Fig. 4, in MazF-transduced CEM-SS cells, HIV-1 replication was effectively suppressed. To more precisely investigate the antiviral effects of MazF, viral production and cell growth were measured every other day after HIV-1 IIIB infection at the MOI of 0.07. As shown in Fig. 2A, in the beginning of the culture from day 0 to day 4, cell growth was similar among CEM-SS cells, MazF-transduced CEM-SS cells, and GFP-transduced CEM-SS cells, as well as uninfected CEM-SS cells. CEM-SS cells harboring the *mazF* (ACA-less) gene grew at a normal rate throughout the time course of HIV-1 IIIB infection, whereas both GFP-transduced CEM-SS cells and the parental cell line showed aberrant growth rates due to HIV-1 infection in late cultures after day 8 (Fig. 2A). Indeed, a high level of p24 was detected in the GFP-transduced cell populations during the course of infection (Fig. 2B). In the case of MazF-transduced cells, however, levels of p24 were three orders of magnitude lower than those of GFP-transduced cells throughout the experiment (Fig. 2B). Notably, CD4 levels of MazF-transduced cells infected with HIV-1 IIIB were largely unaffected (Fig. 3B). Together with the fact that the HIV-1 IIIB infected cells harboring the *mazF* gene grew normally (Fig. 2A), these results suggest that HIV-1 IIIB gene expression in the HIV-1-LTR-regulated *mazF* (ACA-less)-transduced cells is effectively inhibited by blocking HIV-1 replication with little damage to cellular function.
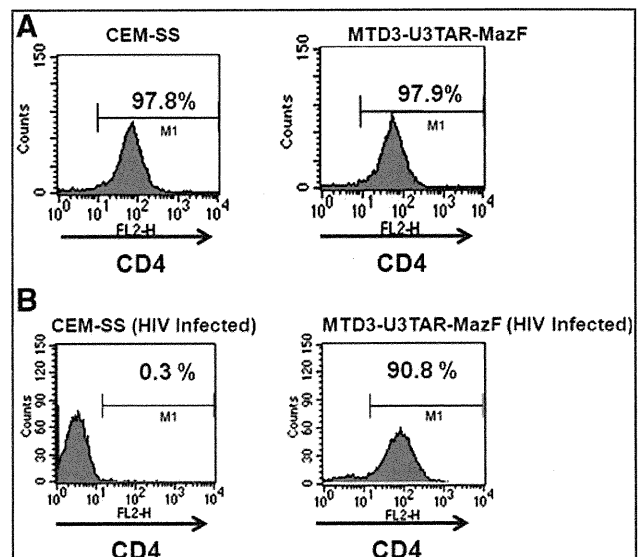

FIG. 3. CD4 levels in MazF-transduced cells. **(A)** Endogenous expression levels of CD4 were analyzed using PE-labeled anti-human CD4 antibody following flow cytometric analysis. **(B)** CEM-SS control cells and CEM-SS cells transduced with MTD3-U3TAR-MazF were infected with HIV-1 IIIB at an MOI of 0.007. After infection, the cells were maintained for 5 weeks and CD4 expression levels were analyzed using PE-labeled anti-human CD4 antibody following flow cytometric analysis.

Next, we examined if HIV-1 IIIB was integrated into the genome of MazF-transduced CEM-SS cells upon HIV-1 infection. Two different regions of the HIV-1 *gag* gene were amplified by PCR using genomic DNA 14 days after HIV-1 IIIB infection. As shown in Fig. 2C, both regions of the *gag* gene were detected in the genome of MazF-transduced CEM-SS cells, which were resistant to HIV-1 replication (lane 3). Similarly, HIV-1 DNA was detected in the genomes of CEM-SS cells (lane 2) and H9-IIIB cells (lane 4) (positive control H9 cells chronically infected with HIV-1 IIIB), whereas no bands were detected in noninfected cells (lane 1). We also established a CEM-SS cell line chronically infected with HIV-1 IIIB (CH-1). When this cell line was mixed with CEM-SS cells or MazF-transduced CEM-SS cells at a ratio of 10, 1, or 0.1%, CEM-SS cells were gradually infected with HIV-1 produced from CH-1 cells (Fig. 2D) and their cell growth was suppressed. Alternatively, MazF-transduced CEM-SS cells showed no growth inhibition (data not shown), indicating that HIV-1 replication was suppressed in MazF-transduced CEM-SS cells. As a result, the culture was eventually taken over by normally growing MazF-transduced CEM-SS cells over the slow-growing CH-1 cells. These data demonstrate that MazF-transduced cells are resistant to HIV-1 IIIB infection by blocking HIV-1 IIIB replication.

To investigate the *mazF* gene expression and subsequent effects more precisely, CEM-SS cells and CEM-SS cells transduced with MTD3-U3TAR-MazF were infected with the Tat-expressing retroviral vectors, M-LTR-Tat-ZG or H-LTR-Tat-ZG (Fig. 5A). Induction of the *mazF* gene in CEM-SS cells transduced with MTD3-U3TAR-MazF was monitored by real-time PCR, and the relative ratios were compared with mock infection (Fig. 5B). Infected cells were also subjected to
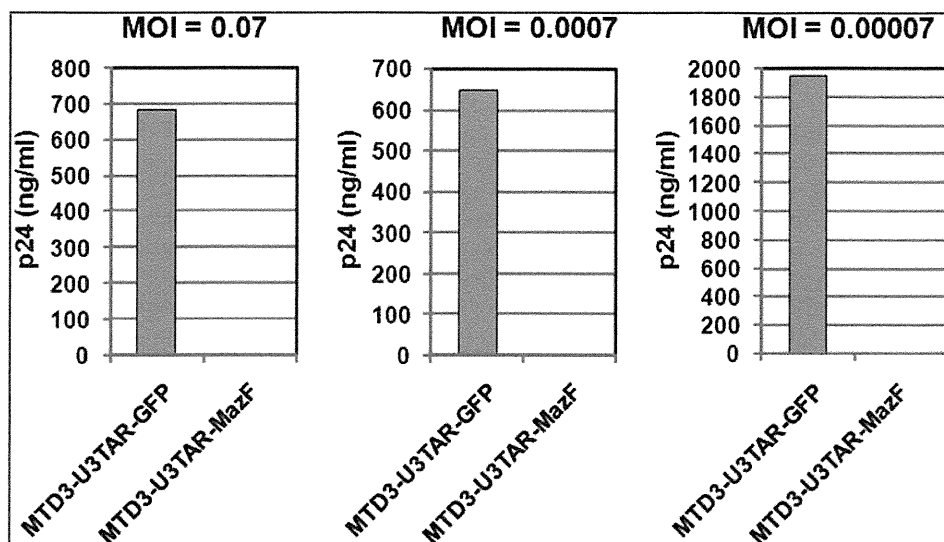
FIG. 4. HIV-1 IIIB infection using MazF-transduced CEM-SS cells at different MOIs. Polyclonal cell populations of CEM-SS resulting from gene transduction with retroviral vectors MTD3-U3TAR-MazF or MTD3-U3TAR-GFP were infected with HIV-1 IIIB at different MOIs (0.07, 0.0007, and 0.00007). Sixteen days after infection, HIV-1 p24 levels in the culture supernatant were estimated using the p24 ELISA kit (PerkinElmer). Given the cytopathic effect of HIV-1, the MTD3-U3TAR-GFP cell population showed delayed proliferation after HIV-1 infection in contrast to the MTD3-U3TAR-MazF population. The delay was more pronounced for the high-MOI group (0.07) than for the low-MOI group (0.00007) at later time points. On day 16 post infection, the accumulated cell number of the high-MOI group was threefold lower than that of the low-MOI group, so the difference in HIV-1 p24 levels between the two MOI groups (0.07 and 0.00007) reflects total cell numbers.

flow cytometry, and both Tat-positive (ZsGreen-positive) cells and dead cells (PI-positive) were monitored (Fig. 5B). As shown in Fig. 5B, strong induction of mazF expression was observed upon constitutive M-LTR-Tat-ZG vector transduction, and there was a significant decline in Tat-positive (ZsGreen-positive) cell population. On the other hand, mazF induction in HIV-LTR-driven Tat expression was lower, and the influence on cell death was also less than by MLV-LTR-driven Tat expression as observed in the PI-positive population. Although these experiments do not directly reflect HIV-1 replication, these data support the hypothesis that only low levels of MazF are expressed upon HIV-1 infection and MazF-positive cells can survive with HIV-1 provirus.

As the SIN-based retroviral vector contains the mazF gene in the normal orientation, the mazF gene is expressed from viral mRNA, resulting in the degradation of the viral RNA and thus significantly reducing the viral titer from this vector. On the other hand, when the MazF expression cassette is
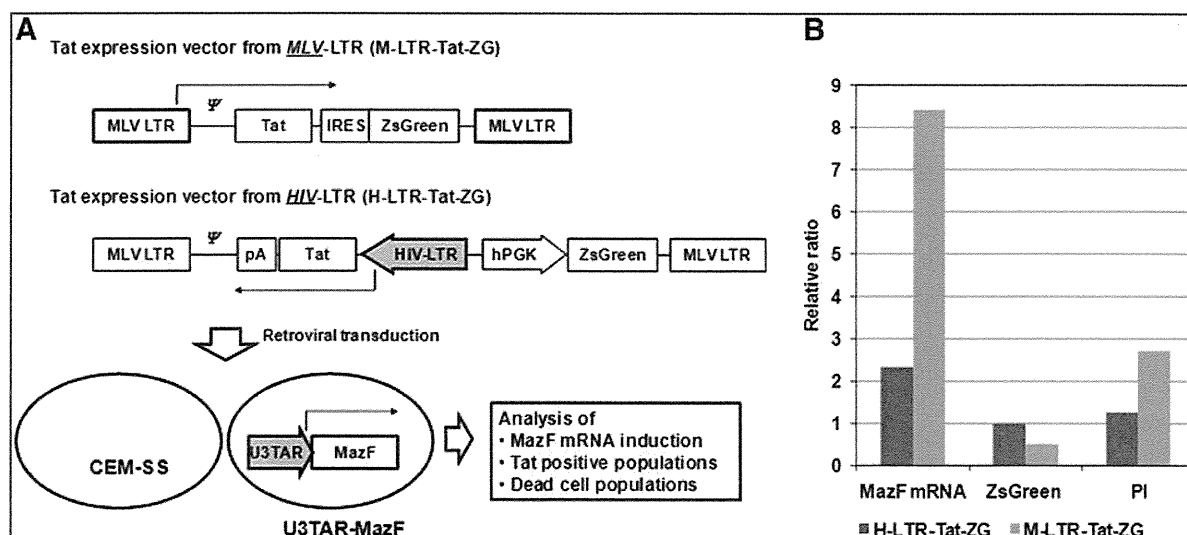

FIG. 5. Analysis of MazF induction upon Tat expression. (A) Outline of experimental procedure to analyze MazF induction upon Tat expression. (B) MazF mRNA levels were analyzed in MTD3-U3TAR-MazF transduced CEM-SS cells after Tat-expressing retroviral vector infection using real-time RT-PCR. The relative fold change is shown compared with that of mock infections. Tat-positive (ZsGreen-positive) cell populations and dead (PI-positive) cell populations in MTD3-U3TAR-MazF-transduced CEM-SS cells were analyzed by flow cytometry 2 days after different Tat retroviral vector transduction. The relative ratio is shown compared with that of CEM-SS cells.

inserted in the opposite direction from the retroviral genome, the viral titer increased and the gene transfer efficiency was improved more than 10 times (data not shown). To investigate the antiviral effect of the TAR-*mazF* system in the primary CD4+ T lymphocytes, the reversely orienting MT-MFR-PL2 vector was introduced into rhesus macaque primary CD4+ T cells from two individual monkeys (#14 and #15). The resulting *mazF*-containing cells were then infected with SIV/HIV-1 chimeric virus SHIV 89.6P. As the SHIV 89.6P harbors HIV-1-derived *env*, *rev*, *vpu*, and *tat* genes, the TAR-*mazF* system is expected to function when MazF-Tmac cells are infected with SHIV 89.6P. Indeed, efficient suppression of SHIV 89.6P replication was observed for both primary cell lines, #14 and #15 (Fig. 6A).

To evaluate further how well the retroviral *mazF* system is able to suppress viral RNA production, total cellular RNAs were extracted from MazF-Tmac cells to estimate quantitatively the amounts of SHIV RNA, as well as the mRNAs for ribosomal protein L13a (RPL13a, XM_001093017) and β-actin (NM_001033084), by real-time PCR. The relative ratios were normalized by using 18S rRNA (FJ436026), which is protected from MazF cleavage in ribosomes (Shimazu et al., 2007). We obtained similar results in MazF-Tmac cells from both #14 and #15 primary cell lines. Representative results from MazF-Tmac cells from #14 are shown in Fig. 6B, where one can see that SHIV RNA was preferentially cleaved, whereas the cellular mRNAs were not affected. These results clearly demonstrate that MazF induction from the Tat system upon SHIV 89.6P infection leads to severe defect in maintaining SHIV 89.6P RNA but does not affect cellular mRNAs in SHIV-infected CD4+ T cells.

Discussion

This study demonstrates the distinct feasibility of RNase-based strategies for gene therapy. RNase-based strategies may be preferred over RNA-based strategies for HIV therapy, because RNases cleave HIV-RNA to cause permanent damage to HIV RNA function. Additionally, as RNases

function as an enzymatic catalyst, they are required only at low concentrations in the cells to effectively block HIV proliferation. In the present study, the gene for MazF, an ACA-specific mRNA interferase, was engineered under the HIV-1 LTR promoter and inserted in the genome of the CD4+ T lymphoid cells so that MazF is expected to be produced only when the cells are infected with HIV-1 to produce the Tat protein. We demonstrated that *mazF*-Tmac cells indeed acquired resistance against SHIV replication, but cell growth was not inhibited after SHIV infection (data not shown), indicating that cellular mRNAs were not significantly affected. Notably, MazF was also able to function against the expression of SHIV proviral genome, because the production of SHIV in the culture supernatant was dramatically reduced.

Acquisition of HIV-1 resistance, and more remarkably the ability of MazF-transduced cells to suppress HIV-1 replication, may be explained as follows: Upon HIV-1 infection, Tat expression is first induced from the HIV-1 proviral genome. Tat then triggers the transcription of the *mazF* gene under the LTR promoter, as well as the full-length HIV proviral genome. The resulting induction of MazF expression leads to the cleavage of newly emerged HIV-1 mRNAs so that Tat protein synthesis is no longer sustainable. However, it is important to note that HIV-1 infection does not hamper cell growth and that the HIV-1 provirus genome is retained in the MazF-transduced cells. Therefore, the cellular level of Tat appears to be maintained at a very low level so that the level of MazF induction is also kept very low enough to cleave HIV-1 mRNAs, but not cellular mRNAs. Depending on the integration site and proviral copy number, there might be some MazF-transduced cells that were not resistant to HIV-1 replication. However, these cells could not survive due to HIV-1-induced cell death.

In mammals, virus infection is known to activate the interferon response to induce RNaseL, which mediates degradation of 28S and 18S ribosomal RNAs. This results in inhibition of protein synthesis as part of the host antiviral response (Silverman, 2003). An amphibian ribonuclease,

FIG. 6. Effect of MazF-induction into rhesus macaque primary CD4+ T cells on SHIV 89.6P replication. (A) Rhesus macaque primary CD4 T cells from two monkeys (#14 and #15) were activated and transduced with MT-MFR-PL2 vector. The MazF-transduced cells (MazF-Tmac cells) were re-activated with CD3/28 beads followed by infection with SHIV 89.6P. On days 3 and 6 post infection, culture supernatants were collected and evaluated for SHIV RNA copy by using the quantitative real-time PCR method. (B) Total cellular RNAs extracted from MazF-Tmac cells at 6 days post SHIV 89.6P infection were used to measure the amounts of SHIV RNA, as well as cellular housekeeping mRNAs, by using the quantitative real-time PCR method.
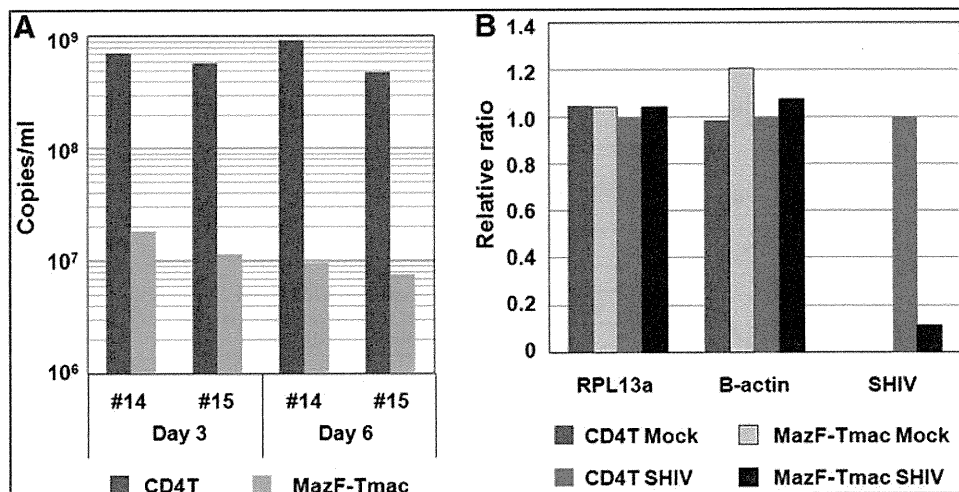
Onconase, is able to inhibit protein synthesis in mammalian cells and has been used as a protein drug. When it was added to the culture media of H9 cells persistently infected with HIV-1, HIV-1 replication was inhibited without blocking cell growth, as degradations of 18S and 28S rRNAs and cellular mRNAs were prevented (Saxena et al., 1996). MazF induction in mammalian cells has shown to cause apoptotic cell death as a result of degradation of cellular mRNAs (Shimazu et al., 2007). However, in the present study, MazF expression induced by HIV-1 Tat appears to be maintained at very low levels, just enough to cleave HIV-1 RNA but not cellular mRNAs, so that cells were able to grow normally. MazF expression may be autoregulated in the cell in such a way that when Tat-induced MazF eliminates invading HIV-1 RNA, Tat expression from the HIV-1 provirus is simultaneously stopped, resulting in simultaneous arrest of MazF production to recover normal cellular functions.

Targeting HIV RNA as a therapeutic strategy using antisense RNA (Levine et al., 2006), ribonucleases (Agarwal et al., 2006), and RNA interference (RNAi) technology (Morris and Rossi, 2004) has been attempted. However, the use of antisense RNA and RNAi technology has not been effective as an anti-HIV technology, as HIV can easily circumvent these RNA inhibitors by creating mutations at the target sequence regions (Lee and Rossi, 2004). On the other hand, the present strategy using MazF targets abundant ACA sequences in HIV-1 RNA (>240), so that it is not possible for HIV-1 to escape from MazF attack by mutations. Furthermore, because MazF has no homology to any mammalian ribonucleases, MazF mRNA interferase activity cannot be inhibited by ribonuclease inhibitors existing in mammalian cells.

In summary, the use of MazF appears to be a novel and highly effective tool for anti-HIV gene therapy. It is effectively able to suppress HIV-1 replication, preventing the emergence of mutated HIV-1. Importantly, MazF induction by invading HIV-1 shows little toxicity to host cells while it efficiently suppresses HIV-1 replication. Specific inhibition of HIV-1 replication by MazF without affecting cell growth is the key feature of MazF-based HIV-1 gene therapy. This may be the first step for RNase-based HIV-1 gene therapy with efficacy in vitro. The feasibility of the MazF-based ex vivo gene therapy may be verified using autologous CD4+ T lymphocytes from HIV-1 patients. To use our mazF vector system for gene therapy, its safety has to be critically evaluated and it should not have any negative impacts on T-cell function. For example, it needs to be shown that there is no alteration in the secretion of functionally important cytokines even though it was observed that MazF expression in HIV-infected CD4+ T cells does not inhibit cell growth. We are currently addressing this question.

Acknowledgments

Author Disclosure Statement

References

Agarwal, S., Nikolai, B., Yamaguchi, T., Lech, P., and Somia N.V. (2006). Construction and use of retroviral vectors encoding the toxic gene barnase. Mol. Ther. 14, 555–563.

Berkhout, B., Silverman, R.H., and Jeang, K.T. (1989). Tat transactivates the human immunodeficiency virus through a nascent RNA target. Cell 59, 273–282.

Kim, S., Ikeuchi, K., Byrn, R., Groopman, J., and Baltimore, D. (1989). Lack of a negative influence on viral growth by the nef gene of human immunodeficiency virus type 1. Proc. Natl. Acad. Sci. U.S.A. 86, 9544–9548.

Lee, J.T., Yu, S.S., Han, E., Kim, S., and Kim, S. (2004). Engineering the splice acceptor for improved gene expression and viral titer in an MLV-based retroviral vector. Gene Ther. 11, 94–99.

Lee, N.S., and Rossi, J.J. (2004). Control of HIV-1 replication by RNA interference. Virus Res. 102, 53–58.

Levine, B.L., Humeau, L.M., Boyer, J., MacGregor, R.R., Rebello, T., Lu, X., Binder, G.K., Slepushkin, V., Lemiale, F., Mascola, J.R., Bushman, F.D., Dropulic, B., and June, C.H. (2006). Gene transfer in humans using a conditionally replicating lentiviral vector. Proc. Natl. Acad. Sci, U.S.A. 103, 17372–17377.

Miyake, A., Ibuki, K., Enose, Y., Suzuki, H., Horiuchi, R., Motohara, M., Saito, N., Nakasone, T., Honda, M., Watanabe, T., Miura, T., and Hayami, M. (2006). Rapid dissemination of a pathogenic simian/human immunodeficiency virus to systemic organs and active replication in lymphoid tissues following intrarectal infection. J. Gen. Virol. 87, 1311–1320.

Morris, K.V., and Rossi, J.J. (2006). Lentivirus-mediated RNA interference therapy for human immunodeficiency virus type 1 infection. Hum. Gene Ther. 17, 479–486.

Nariya, H., and Inouye, M. (2008). MazF, an mRNA interferase, mediates programmed cell death during multicellular Myxococcus development. Cell 132, 55–66.

Reimann, K.A., Li, J.T., Voss, G., Lekutis, C., Tenner-Racz, K., Racz, P., Lin, W., Montefiori, D.C., Lee-Parritz, D.E., Lu, Y., Collman, R.G., Sodroski, J., and Letvin, N.L. (1996). An env gene derived from a primary human immunodeficiency virus type 1 isolate confers high in vivo replicative capacity to a chimeric simian/human immunodeficiency virus in rhesus monkeys. J. Virol. 70, 3198–3206.

Saxena, S.K., Gravell, M., Wu, Y.N., Mikulski, S.M., Shogen, K., Ardelt, W., and Youle, R.J. (1996). Inhibition of HIV-1 production and selective degradation of viral RNA by an amphibian ribonuclease. J. Biol. Chem. 271, 20783–20788.

Shimazu, T., Degenhardt, K., Nur-E-Kamal, A., Zhang, J., Yoshida, T., Zhang, Y., Mathew, R., White, E., and Inouye, M. (2007). NBK/BIK antagonizes MCL-1 and BCL-XL and activates BAK-mediated apoptosis in response to protein synthesis inhibition. Genes Dev. 21, 929–941.

Silverman, R.H. (2003). Implications for RNase L in prostate cancer biology. Biochemistry 42, 1805–1812.

Verzeletti, S., Bonini, C., Marktel, S., Nobili, N., Ciceri, F., Traversari, C., and Bordignon, C. (1998). Herpes simplex virus thymidine kinase gene transfer for controlled graft-versus-host disease and graft-versus-leukemia: clinical follow-up and improved new vectors. Hum. Gene Ther. 9, 2243–2251.

Yamaguchi, Y., and Inouye, M. (2009). mRNA interferases, sequence-specific endoribonucleases from the toxin-antitoxin systems. Prog. Mol. Biol. Transl. Sci. 85, 467–500.

Yu, S.F., von Rüden, T., Kantoff, P.W., Garber, C., Seiberg, M., Rüther, U., Anderson, W.F., Wagner, E.F., and Gilboa, E.

(1986). Self-inactivating retroviral vectors designed for transfer of whole genes into mammalian cells. Proc. Natl. Acad. Sci. U.S.A. 83, 3194–3198.

Yu, S.S., Han, E., Hong, Y., Lee, J.T., Kim, S., and Kim, S. (2003). Construction of a retroviral vector production system with the minimum possibility of a homologous recombination. Gene Ther. 10, 706–711.

Zhang, Y., Zhang, J., Hoeflich, K.P., Ikura, M., Qing, G., and Inouye, M. (2003). MazF cleaves cellular mRNAs specifically at ACA to block protein synthesis in *Escherichia coli*. Mol. Cell 12, 913–923.

Zhu, L., Zhang, Y., The, J.S., Zhang, J., Connell, N., Rubin, H., and Inouye, M. (2006). Characterization of mRNA interferases from Mycobacterium tuberculosis. J. Biol. Chem. 281, 18638–18643.

Zhu, L., Inoue, K., Yoshizumi, S., Kobayashi, H., Zhang, Y., Ouyang, M., Kato, F., Sugai, M., and Inouye, M. (2009). *Staphylococcus aureus* MazF specifically cleaves a pentad sequence, UACAU, which is unusually abundant in the mRNA for pathogenic adhesive factor SraP. J. Bacteriol. 191, 3248–3255.

Address correspondence to:
Dr. Ikunoshin Kato
Center for Cell and Gene Therapy
Takara Bio Inc.
Seta 3-4-1
Otsu, Shiga
520-2193, Japan

E-mail: ikukatiku@zeus.eonet.ne.jp

Dr. Masayori Inouye
Department of Biochemistry
Robert Wood Johnson Medical School
675 Hoes Lane
Piscataway, NJ 08854, USA

E-mail: inouye@umdnj.edu